Formulation for zirconia toughened alumina (ZTA) reinforced metal matrix composites based on a three-phase concentric inclusion model

Jiyang Yan[1], Lifeng Ma[*1,2] , Juan Wang[*3]

1. S&V Lab, Department of Engineering Mechanics, Xi'an Jiaotong University, 710049 Xi'an, China
2. Department of Mechanical, Materials and Manufacturing Engineering, University of Nottingham, University Park, NG7 2RD, UK
3. Institute of New Materials, Guangdong Academy of Sciences, National Engineering Research Center of Powder Metallurgy of Titanium & Rare Metals, Guangdong Provincial Key Laboratory of Metal Toughening Technology and Application, Guangzhou, 510650, China

Abstract

In this paper, a model of a coated inhomogeneous circular inclusion concentrically embedded within a finite matrix is proposed, which is employed to analyze zirconia toughened alumina (ZTA) reinforced metal matrix composites. The general solution is derived based on the equivalent eigenstrain principle and the superposition principle. Then, the model is used to study the influence of the thermal strains due to temperature changes on the stress distribution in the composite. Also, a particular composite, ZTA reinforced high chromium cast iron (HCCI), is exemplified, and the normalized stress distribution is given. In addition, the toughening mechanism associated with the transformation of zirconia is discussed. The above results help to estimate the stress level of ZTA reinforced metal composites. This three-phase concentric inclusion model is expected to be used to the structure design of composite materials.

Keywords: Three-phase inhomogeneous concentric inclusion; Finite matrix; Zirconia toughened alumina; Transformation toughening.

1. Introduction

Over the past few decades, ceramic particles reinforced metal matrix composites have become a class of superior materials in terms of impact erosion resistance, wear resistance, fatigue, and fracture properties (Fernie *et al.*, 2009; Harris, 1988; Li *et al.*, 2007; Miracle, 2005; Pagounis and Lindroos, 1998). Among numerous ceramic materials, research on zirconia toughened alumina (ZTA) has been through a dramatic increase due to its excellent strength and high toughness since the transformation

* Corresponding authors.

Email: malf@mail.xjtu.edu.cn (L.M.); wangjuan@gdinm.com (J.W.), Tel.: +44 07542 773061

toughening of zirconia was first reported by Garvie *et al.* (1975). Then in the late 1970s and the 1980s, the transformation toughening mechanism of zirconia and the microstructure in ZTA were basically identified with great intelligence and energy devoted. Related overviews of references can be found in Hannink *et al.* (2000), Wang and Stevens (1989), and Heuer (1987). The existence of ZTA in metal matrix materials can significantly increase the wear resistance of the entire composites, which have been considered as emerging alternatives for traditional wear-resistant materials (Hill *et al.*, 2011; Kambakas and Tsakiropoulos, 2005; Ma *et al.*, 2018; Qiu *et al.*, 2017; Ru *et al.*, 2017; Wang *et al.*, 2020; Zheng *et al.*, 2014). However, due to the complex microstructure and the inhomogeneity of different components, it is difficult to evaluate the internal stress states and the transformation toughening of zirconia in ZTA reinforced metal matrix composites. And this explains, to some extent, why the studies on ZTA reinforced metal matrix composites are mainly focused on the improvement of preparation technologies (Ma *et al.*, 2019; Qiu *et al.*, 2019; Ru *et al.*, 2019a; Tang *et al.*, 2014; Wang *et al.*, 2020), the characterization and microstructure of interfacial transition zone (He *et al.*, 2022; Li *et al.*, 2019, 2022; Qin *et al.*, 2022; Sui *et al.*, 2018; Zhou *et al.*, 2019), and the modification of ZTA (Fan *et al.*, 2018; Gao *et al.*, 2022; Ru *et al.*, 2017; Ru *et al.*, 2019b; Wang *et al.*, 2022; Zeng *et al.*, 2021) at present.

The microstructure of ZTA shows that dispersed zirconia particles are wrapped within alumina particles, as shown in Fig. 1a. Then dispersed ZTA particles are coated with matrix materials in ZTA reinforced metal matrix composites, as shown in Fig. 1b. As a result, the elastic response and phase transitions of zirconia are actually controlled by the alumina and matrix materials. Considering above mentioned, a three-phase concentric inclusion model, in which the zirconia is coated with the alumina layer and embedded within the metal matrix, is established as a representative volume element to study the mechanical behavior in ZTA reinforced metal matrix composites, as shown in Fig. 2. It is worth noting that the model is formed in a plane strain configuration and it is a generalized model, so no specific parameters (material properties, for instance) are designated at first. The three-phase concentric inclusion model could offer distinct advantages as follows: (*i*) The stress distributions can be directly calculated, which helps to estimate the stress levels of composites and avoid extremely high-stress levels without preparation of composite materials and instrumental measurement. (*ii*) With known stress states, it is capable of assessing the phase transformation strain of zirconia as stress-induced transformation toughening is one of the well-accepted toughening

mechanisms for ZTA ceramics. (*iii*) The matrix materials and the proportion of components can be any value, so that the model can also be employed to design the composites with better overall performance.

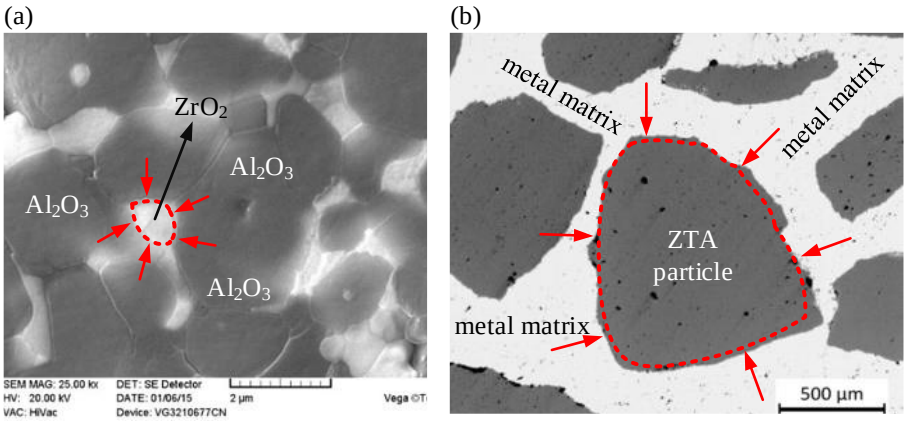

Fig. 1 The microstructure of ZTA reinforced metal matrix composites. (a) A scanning electron micrograph of ZTA showing that ZrO_2 particles are bounded by surrounding Al_2O_3 particles. (b) An optical micrograph showing ZTA particles surrounded by the metal matrix.

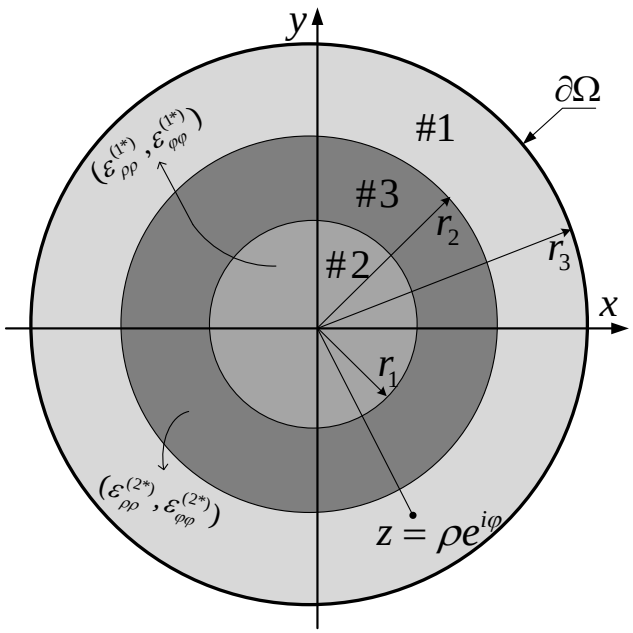

Fig. 2 A model of coated circular inhomogeneous inclusion concentrically embedded within a finite matrix: $\partial\Omega$ represents the boundary of the model, inhomogeneous materials $\#2$ and $\#3$ reside in the domains $\rho < r_1$ and $r_1 < \rho < r_2$, respectively, and the matrix material $\#1$ is distributed in the region $r_2 < \rho < r_3$. The interfaces between different materials are perfectly bonded. $\varepsilon_{\rho\rho}^{(1*)}(\varepsilon_{\rho\rho}^{(2*)})$ and $\varepsilon_{\varphi\varphi}^{(1*)}(\varepsilon_{\varphi\varphi}^{(2*)})$ are

independent non-uniform radial and hoop eigenstrains distributed in #2(#3).

The three-phase concentric inhomogeneous inclusion within an infinite matrix has been investigated by us (Yan *et al.*, 2022). However, the analytical solutions cannot be directly employed in this paper because the size of inclusions can sometimes be recognized as relatively large compared with the size of the matrix. ZTA particles could account for a large proportion of ZTA reinforced metal composites, and the content of ZTA has a great influence on the mechanical properties of the composites (Xue *et al.*, 2019; Zheng *et al.*, 2014, 2019). Therefore, the mechanical model should be modified to satisfy application scenarios under the finite matrix based on the equivalent eigenstrain principle (Ma and Korsunsky, 2014, 2022; Wang *et al.*, 2020) and the superposition principle. Specific procedures are organized as follows. A homogeneous inclusion problem in a finite matrix can be solved by decomposing it into the homogeneous inclusion problem embedded in an infinite matrix and the auxiliary boundary problem of the corresponding finite matrix subjected to the load determined by the former problem shown in Fig. 3. Then, with the equivalent eigenstrain principle, an inhomogeneous inclusion problem (the three-phase concentric inclusion problem) within a finite matrix can be transformed into a corresponding homogeneous one (the coated circular homogeneous inclusion problem), as shown in Fig. 4. The total strain and stress fields remain the same after the transformation. Finally, we can figure out the three-phase concentric inhomogeneous inclusion problem since the transformed homogeneous one is solved.

The present study aims to simulate the microstructure of ZTA reinforced metal matrix composites with a representative volume element, in which the non-uniform axisymmetric radial and hoop eigenstrains are independently distributed in the circular and annular zones, as shown in Fig. 2. The stress distributions for the entire inclusion system are to be derived. In specific cases, materials #1, #2, and #3 are designated as the metal matrix, zirconia, and alumina separately and eigenstrains are referred to as thermal strains or transformation strains. Furthermore, analytical solutions are employed to estimate stress levels and the transformation degree of zirconia.

The paper is constructed as follows: the analytical solution of the coated circular homogeneous inclusion problem in a finite matrix is given in §2. Then based on the solution obtained in §2, the analytical solution of the three-phase concentric inclusion problem is provided in §3. In §4, the model with appropriate eigenstrains caused by

thermal load is investigated. The model is subsequently employed with specific material properties to study stress distributions and the transformation of zirconia in §5. Finally, some conclusions are drawn, and possible extensions of the model are discussed in §6.

2. Analytical solution for the coated circular *homogeneous* inclusion in a finite matrix

In this section, the coated circular homogeneous inclusion problem in a finite matrix will be investigated based on our previous work (Yan *et al.*, 2022) and the superposition principle. The analytical solution plays an important role in solving corresponding inhomogeneous inclusion problem in §3.

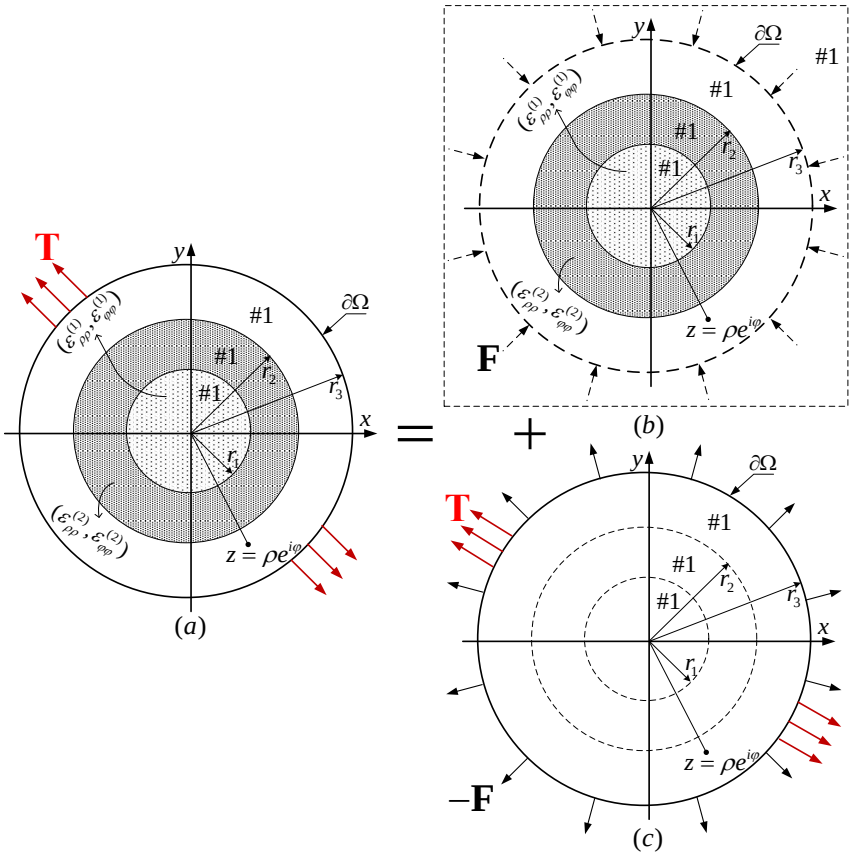

Fig. 3 The superposition principle for the coated circular homogeneous inclusion system. $\mathbf{T}$ is the boundary load. The original problem (Fig. 3a) is decomposed into the homogeneous inclusion problem (Fig. 3b) embedded in an infinite matrix and the auxiliary boundary problem (Fig. 3c). $\mathbf{F} = [F_n, F_t]^T$ is the traction along the boundary $\partial\Omega$ determined by the stress distribution of Fig. 3b with the free-body diagram method. F_n and F_t represent the normal and tangential tractions.

The model of the coated circular homogeneous inclusion is shown in Fig. 3a. The materials in the circular and annular zones share the same property with the matrix, and we suppose that the non-uniform axisymmetric eigenstrains are known as

$$\boldsymbol{\varepsilon}^{(1)}=\begin{cases}\varepsilon_{\varphi\varphi}^{(1^*)}=\varepsilon_{\varphi\varphi}^{(1)}(r)\\ \varepsilon_{\rho\rho}^{(1^*)}=\varepsilon_{\rho\rho}^{(1)}(r)\ ,(0<r<r_1)\\ \varepsilon_{\rho\varphi}^{(1^*)}=0\end{cases},\qquad \boldsymbol{\varepsilon}^{(2)}=\begin{cases}\varepsilon_{\varphi\varphi}^{(2^*)}=\varepsilon_{\varphi\varphi}^{(2)}(r)\\ \varepsilon_{\rho\rho}^{(2^*)}=\varepsilon_{\rho\rho}^{(2)}(r)\ ,(r_1\le r\le r_2)\\ \varepsilon_{\rho\varphi}^{(2^*)}=0\end{cases} \tag{2.1}$$

where $\varepsilon_{\rho\rho}^{(1^*)}$, $\varepsilon_{\varphi\varphi}^{(1^*)}$, $\varepsilon_{\rho\rho}^{(2^*)}$ and $\varepsilon_{\varphi\varphi}^{(2^*)}$ represent the eigenstrain; $\varepsilon_{\rho\rho}^{(1)}$, $\varepsilon_{\varphi\varphi}^{(1)}$, $\varepsilon_{\rho\rho}^{(2)}$ and $\varepsilon_{\varphi\varphi}^{(2)}$ are known distribution. With the superposition principle, in the homogeneous inclusion system Fig. 3a, the total strain is aroused by eigenstrains (i.e. $\boldsymbol{\varepsilon}^{(1)}$ and $\boldsymbol{\varepsilon}^{(2)}$) and the boundary load $\mathbf{T}$, and the actual stress $\boldsymbol{\sigma}^{(a)}$ can be decomposed into $\boldsymbol{\sigma}^{(b)}$ and $\boldsymbol{\sigma}^{(c)}$. $\boldsymbol{\sigma}^{(b)}$ is the stress distribution caused by eigenstrains in an infinite matrix as shown in Fig. 3b. $\boldsymbol{\sigma}^{(c)}$ is the stress distribution caused by the boundary tractions $-\mathbf{F}$ and $\mathbf{T}$ as shown in Fig. 3c. Through the boundary conditions at $\rho=r_3$ in Fig. 3b, we can get $\mathbf{F}$ with the free-body diagram method as

$$\mathbf{F}=\begin{bmatrix}F_n\\ F_t\end{bmatrix}=\begin{bmatrix}\sigma_{\rho\rho}^{(b)}n_1+\sigma_{\rho\varphi}^{(b)}n_2\\ \sigma_{\rho\varphi}^{(b)}n_1+\sigma_{\varphi\varphi}^{(b)}n_2\end{bmatrix}, \tag{2.2}$$

where n_1 and n_2 are cosine and sine of angle between exterior unit normal vector of the boundary $\partial\Omega$ and the x-axis when the x-axis and the ρ-axis coincide, which means $n_1=1, n_2=0$. And $\boldsymbol{\sigma}^{(c)}$ satisfies the boundary conditions on $\partial\Omega$ as

$$\boldsymbol{\sigma}^{(c)}\big|_{\partial\Omega}=-\mathbf{F}+\mathbf{T}. \tag{2.3}$$

As mentioned above, the stress for the homogeneous inclusion system in a finite matrix (see, Fig. 3a) can be decomposed into two parts, which is shown in Fig. 3b and Fig. 3c. For the homogeneous inclusion system in an infinite matrix, the stress distribution ($\boldsymbol{\sigma}^{(b)}$) was derived by us (Yan *et al.*, 2022) as

$$\boldsymbol{\sigma}^{(b)}=\begin{cases}\sigma_{\rho\rho}^{(b)}=-\dfrac{4\mu_1}{(1+\kappa_1)}\dfrac{1}{\rho^2}\left[\int_0^{r_1}\left(\varepsilon_{\varphi\varphi}^{(1)}+\varepsilon_{\rho\rho}^{(1)}\right)rdr+\int_{r_1}^{r_2}\left(\varepsilon_{\varphi\varphi}^{(2)}+\varepsilon_{\rho\rho}^{(2)}\right)rdr\right]\\ \sigma_{\varphi\varphi}^{(b)}=\dfrac{4\mu_1}{(1+\kappa_1)}\dfrac{1}{\rho^2}\left[\int_0^{r_1}\left(\varepsilon_{\varphi\varphi}^{(1)}+\varepsilon_{\rho\rho}^{(1)}\right)rdr+\int_{r_1}^{r_2}\left(\varepsilon_{\varphi\varphi}^{(2)}+\varepsilon_{\rho\rho}^{(2)}\right)rdr\right] \quad ,\rho>r_2\\ \sigma_{\rho\varphi}^{(b)}=0\end{cases}, \text{(2.4a)}$$

$$\boldsymbol{\sigma}^{(b)}=\begin{cases}\sigma_{\rho\rho}^{(b)}=\dfrac{4\mu_1}{(1+\kappa_1)}\left[\int_\rho^{r_1}\dfrac{\varepsilon_{\varphi\varphi}^{(1)}-\varepsilon_{\rho\rho}^{(1)}}{r}dr+\int_{r_1}^{r_2}\dfrac{\varepsilon_{\varphi\varphi}^{(2)}-\varepsilon_{\rho\rho}^{(2)}}{r}dr-\dfrac{1}{\rho^2}\int_0^{\rho}\left(\varepsilon_{\varphi\varphi}^{(1)}+\varepsilon_{\rho\rho}^{(1)}\right)rdr\right]\\ \sigma_{\varphi\varphi}^{(b)}=\dfrac{4\mu_1}{(1+\kappa_1)}\left[\int_\rho^{r_1}\dfrac{\varepsilon_{\varphi\varphi}^{(1)}-\varepsilon_{\rho\rho}^{(1)}}{r}dr+\int_{r_1}^{r_2}\dfrac{\varepsilon_{\varphi\varphi}^{(2)}-\varepsilon_{\rho\rho}^{(2)}}{r}dr+\dfrac{1}{\rho^2}\int_0^{\rho}\left(\varepsilon_{\varphi\varphi}^{(1)}+\varepsilon_{\rho\rho}^{(1)}\right)rdr-2\varepsilon_{\varphi\varphi}^{(1)}\right],(\rho<r_1)\\ \sigma_{\rho\varphi}^{(b)}=0\end{cases}$$

, (2.4b)

$$\boldsymbol{\sigma}^{(b)}=\begin{cases}\sigma_{\rho\rho}^{(b)}=\dfrac{4\mu_1}{(1+\kappa_1)}\left[\begin{array}{l}\displaystyle\int_\rho^{r_2}\frac{\varepsilon_{\varphi\varphi}^{(2)}-\varepsilon_{\rho\rho}^{(2)}}{r}dr-\frac{1}{\rho^2}\int_0^{r_1}\left(\varepsilon_{\varphi\varphi}^{(1)}+\varepsilon_{\rho\rho}^{(1)}\right)rdr\\ \displaystyle-\frac{1}{\rho^2}\int_{r_1}^{\rho}\left(\varepsilon_{\varphi\varphi}^{(2)}+\varepsilon_{\rho\rho}^{(2)}\right)rdr\end{array}\right]\\ \sigma_{\varphi\varphi}^{(b)}=\dfrac{4\mu_1}{(1+\kappa_1)}\left[\begin{array}{l}\displaystyle\int_\rho^{r_2}\frac{\varepsilon_{\varphi\varphi}^{(2)}-\varepsilon_{\rho\rho}^{(2)}}{r}dr+\frac{1}{\rho^2}\int_0^{r_1}\left(\varepsilon_{\varphi\varphi}^{(1)}+\varepsilon_{\rho\rho}^{(1)}\right)rdr\\ \displaystyle+\frac{1}{\rho^2}\int_{r_1}^{\rho}\left(\varepsilon_{\varphi\varphi}^{(2)}+\varepsilon_{\rho\rho}^{(2)}\right)rdr-2\varepsilon_{\varphi\varphi}^{(2)}\end{array}\right],(r_1\le\rho\le r_2)\\ \sigma_{\rho\varphi}^{(b)}=0\end{cases}, \text{(2.4c)}$$

where $\kappa_i\left(i=1,2,3\right)$ are Kolosov's constants, $\kappa=3-4\nu$ for plane strain and $\kappa=\left(3-\nu\right)/\left(1+\nu\right)$ for plane stress; $\mu_i(i=1,2,3)$ are shear moduli and ν represents poisson's ratio. In Fig. 3c, for the specific boundary value problem ($\mathbf{T}=0$), the stress distribution $\boldsymbol{\sigma}^{(c)}$ is totally aroused by the boundary traction $-\mathbf{F}$. And $\mathbf{F}$ can be derived with Eq. (2.2) and (2.4a) as

$$\begin{cases} F_n = \sigma^i_{\rho\rho}\big|_{\rho=r_2} = -\dfrac{4\mu_1}{(1+\kappa_1)}\dfrac{1}{r_3^2}\left[\int_0^{r_1}\left(\varepsilon^{(1)}_{\varphi\varphi}+\varepsilon^{(1)}_{\rho\rho}\right)r dr + \int_{r_1}^{r_2}\left(\varepsilon^{(2)}_{\varphi\varphi}+\varepsilon^{(2)}_{\rho\rho}\right)r dr\right] \\ F_t = 0 \end{cases}. \quad (2.5)$$

Then the stress distribution $\boldsymbol{\sigma}^{(c)}$ induced by $-\mathbf{F}$ in Fig. 3c can be expressed as

$$\boldsymbol{\sigma}^{(c)} = \begin{cases} \sigma^{(c)}_{\rho\rho} = \dfrac{4\mu_1}{(1+\kappa_1)}\dfrac{1}{r_3^2}\left[\int_0^{r_1}\left(\varepsilon^{(1)}_{\varphi\varphi}+\varepsilon^{(1)}_{\rho\rho}\right)r dr + \int_{r_1}^{r_2}\left(\varepsilon^{(2)}_{\varphi\varphi}+\varepsilon^{(2)}_{\rho\rho}\right)r dr\right] \\ \sigma^{(c)}_{\varphi\varphi} = \dfrac{4\mu_1}{(1+\kappa_1)}\dfrac{1}{r_3^2}\left[\int_0^{r_1}\left(\varepsilon^{(1)}_{\varphi\varphi}+\varepsilon^{(1)}_{\rho\rho}\right)r dr + \int_{r_1}^{r_2}\left(\varepsilon^{(2)}_{\varphi\varphi}+\varepsilon^{(2)}_{\rho\rho}\right)r dr\right] \\ \sigma^{(c)}_{\rho\varphi} = 0 \end{cases}. \quad (2.6)$$

It is not difficult to see that the expressions in Eq. (2.6) are constants. For convenience in subsequent derivation, we denote

$$A = \frac{4\mu_1}{(1+\kappa_1)}\frac{1}{r_3^2}\left[\int_0^{r_1}\left(\varepsilon^{(1)}_{\varphi\varphi}+\varepsilon^{(1)}_{\rho\rho}\right)r dr + \int_{r_1}^{r_2}\left(\varepsilon^{(2)}_{\varphi\varphi}+\varepsilon^{(2)}_{\rho\rho}\right)r dr\right]. \quad (2.7)$$

Then by superposing Eqs. (2.4) and (2.6), the stress $\boldsymbol{\sigma}^{(a)}$ can be obtained as

$$\boldsymbol{\sigma}^{(a)} = \begin{cases} \sigma_{\rho\rho} = -\dfrac{Ar_3^2}{\rho^2} + A \\ \sigma_{\varphi\varphi} = \dfrac{Ar_3^2}{\rho^2} + A \quad ,(r_2 < \rho \le r_3), \\ \sigma_{\rho\varphi} = 0 \end{cases} \quad (2.8a)$$

$$\boldsymbol{\sigma}^{(a)} = \begin{cases} \sigma^{(1)}_{\rho\rho} = \dfrac{4\mu_1}{(1+\kappa_1)}\left[\begin{array}{l}\displaystyle\int_\rho^{r_1}\frac{\varepsilon^{(1)}_{\varphi\varphi}-\varepsilon^{(1)}_{\rho\rho}}{r}dr + \int_{r_1}^{r_2}\frac{\varepsilon^{(2)}_{\varphi\varphi}-\varepsilon^{(2)}_{\rho\rho}}{r}dr \\ \displaystyle -\frac{1}{\rho^2}\int_0^\rho\left(\varepsilon^{(1)}_{\varphi\varphi}+\varepsilon^{(1)}_{\rho\rho}\right)r dr\end{array}\right] + A \\ \sigma^{(1)}_{\varphi\varphi} = \dfrac{4\mu_1}{(1+\kappa_1)}\left[\begin{array}{l}\displaystyle\int_\rho^{r_1}\frac{\varepsilon^{(1)}_{\varphi\varphi}-\varepsilon^{(1)}_{\rho\rho}}{r}dr + \int_{r_1}^{r_2}\frac{\varepsilon^{(2)}_{\varphi\varphi}-\varepsilon^{(2)}_{\rho\rho}}{r}dr \\ \displaystyle +\frac{1}{\rho^2}\int_0^\rho\left(\varepsilon^{(1)}_{\varphi\varphi}+\varepsilon^{(1)}_{\rho\rho}\right)r dr - 2\varepsilon^{(1)}_{\varphi\varphi}\end{array}\right] + A \ ,(\rho < r_1), \\ \sigma^{(1)}_{\rho\varphi} = 0 \end{cases} \quad (2.8b)$$

$$\boldsymbol{\sigma}^{(a)}=\begin{cases}\sigma_{\rho\rho}^{(2)}=\dfrac{4\mu_1}{(1+\kappa_1)}\left[\begin{array}{l}\displaystyle\int_{\rho}^{r_2}\frac{\varepsilon_{\varphi\varphi}^{(2)}-\varepsilon_{\rho\rho}^{(2)}}{r}dr-\frac{1}{\rho^2}\int_0^{r_1}\left(\varepsilon_{\varphi\varphi}^{(1)}+\varepsilon_{\rho\rho}^{(1)}\right)rdr\\ \displaystyle-\frac{1}{\rho^2}\int_{r_1}^{\rho}\left(\varepsilon_{\varphi\varphi}^{(2)}+\varepsilon_{\rho\rho}^{(2)}\right)rdr\end{array}\right]+A\\ \sigma_{\varphi\varphi}^{(2)}=\dfrac{4\mu_1}{(1+\kappa_1)}\left[\begin{array}{l}\displaystyle\int_{\rho}^{r_2}\frac{\varepsilon_{\varphi\varphi}^{(2)}-\varepsilon_{\rho\rho}^{(2)}}{r}dr+\frac{1}{\rho^2}\int_0^{r_1}\left(\varepsilon_{\varphi\varphi}^{(1)}+\varepsilon_{\rho\rho}^{(1)}\right)rdr\\ \displaystyle+\frac{1}{\rho^2}\int_{r_1}^{\rho}\left(\varepsilon_{\varphi\varphi}^{(2)}+\varepsilon_{\rho\rho}^{(2)}\right)rdr-2\varepsilon_{\varphi\varphi}^{(2)}\end{array}\right]+A\ ,(r_1\le\rho\le r_2)\ .\\ \sigma_{\rho\varphi}^{(2)}=0\end{cases}$$

(2.8c)

Eq. (2.8) is the analytical solution for the original problem shown in Fig. 3a. If the matrix becomes infinite (i.e. $r_3\to+\infty$), it can be easily seen that A degenerates into zero, and Eq. (2.8) will convert to the stress distribution of an infinite matrix automatically. This may partially validate the previous manipulation.

In this section, the stress distribution for the coated circular homogeneous inclusion in a finite matrix is obtained with known eigenstrains. In the next section, we will investigate the corresponding inhomogeneous inclusion system based on the analytical solution obtained in this section.

3. Analytical solution for the three-phase concentric *inhomogeneous* inclusion in a finite matrix

In this section, the analytical solution for a coated circular inhomogeneous inclusion concentrically embedded within a finite matrix will be derived based on the result in §2 and the equivalent eigenstrain principle (Ma and Korsunsky, 2014, 2022; Wang *et al.*, 2020). Non-uniform eigenstrains exist in the circular and annular zones, and the matrix is eigenstrain-free, as shown in Fig. 4a. The interfaces between materials are assumed to be perfectly bonded. The eigenstrain distributions are given as follows:

$$\begin{cases} \varepsilon_{\varphi\varphi}^{(1^*)} = f_1(\rho) \\ \varepsilon_{\rho\rho}^{(1^*)} = f_2(\rho)\ ,(0<\rho<r_1) \\ \varepsilon_{\rho\varphi}^{(1^*)} = 0 \end{cases}, \quad \begin{cases} \varepsilon_{\varphi\varphi}^{(2^*)} = f_3(\rho) \\ \varepsilon_{\rho\rho}^{(2^*)} = f_4(\rho)\ ,(r_1\le\rho\le r_2) \\ \varepsilon_{\rho\varphi}^{(2^*)} = 0 \end{cases} \tag{3.1}$$

in which, $f_1(\rho)$, $f_2(\rho)$, $f_3(\rho)$, and $f_4(\rho)$ are supposed already known.

3.1. The equivalent eigenstrain principle for inhomogeneous inclusion problems

According to the equivalent eigenstrain principle (Ma and Korsunsky, 2014, 2022; Wang *et al.*, 2020), an inhomogeneous inclusion system with initial eigenstrain distributions (Fig. 4a) can be solved by transforming it into a corresponding homogeneous inclusion system with new eigenstrain distributions (Fig. 4b). The unknown transformed eigenstrains (also equivalent eigenstrains) should secure that the two inclusion systems (a) and (b) share the same total strain and stress fields. The transform equations can be expressed as:

$$\boldsymbol{\sigma} = \begin{cases} \mathbf{C}_1(\boldsymbol{\varepsilon}-\boldsymbol{\varepsilon}^{(1)}) = \mathbf{C}_2(\boldsymbol{\varepsilon}-\boldsymbol{\varepsilon}^{(1^*)}) & \mathbf{x}\in\Omega_2(\#2) \\ \mathbf{C}_1(\boldsymbol{\varepsilon}-\boldsymbol{\varepsilon}^{(2)}) = \mathbf{C}_3(\boldsymbol{\varepsilon}-\boldsymbol{\varepsilon}^{(2^*)}) & \mathbf{x}\in\Omega_3(\#3)\ , \\ \mathbf{C}_1\boldsymbol{\varepsilon}=\mathbf{C}_1\boldsymbol{\varepsilon} & \mathbf{x}\in\Omega_1(\#1) \end{cases} \tag{3.2}$$

in which, Ω_1, Ω_2, and Ω_3 denotes the matrix area, the circular zone, and the annular zone, respectively; $\mathbf{C_1}$, $\mathbf{C_2}$, and $\mathbf{C_3}$ are elastic constants of the matrix ($\#1$), the core ($\#2$), and the annular ($\#3$), respectively; $\boldsymbol{\sigma}$ and $\boldsymbol{\varepsilon}$ are the total strain and stress; $\boldsymbol{\varepsilon}^{(1)}$ and $\boldsymbol{\varepsilon}^{(2)}$ are equivalent eigenstrains distributed in the circular and annular zones after transformation, respectively. And the equivalent eigenstrains can be calculated with the expression of the total strain derived from Eq. (3.2) as

$$\boldsymbol{\varepsilon} = \begin{cases} \mathbf{C}_1^{-1}\boldsymbol{\sigma}^{(1)} + \boldsymbol{\varepsilon}^{(1)} = \mathbf{C}_2^{-1}\boldsymbol{\sigma}^{(1)} + \boldsymbol{\varepsilon}^{(1^*)} & ,\mathbf{x}\in\Omega_2 \\ \mathbf{C}_1^{-1}\boldsymbol{\sigma}^{(2)} + \boldsymbol{\varepsilon}^{(2)} = \mathbf{C}_3^{-1}\boldsymbol{\sigma}^{(2)} + \boldsymbol{\varepsilon}^{(2^*)} & ,\mathbf{x}\in\Omega_3 \end{cases}. \tag{3.3}$$

In Eq. (3.3), $\boldsymbol{\sigma}^{(1)}$ and $\boldsymbol{\sigma}^{(2)}$ are stress distributions within the circular and annular zones, which have been derived in Eq. (2.8) and both of them can be expressed as functions of $\boldsymbol{\varepsilon}^{(1)}$ and $\boldsymbol{\varepsilon}^{(2)}$. $\boldsymbol{\varepsilon}^{(1^*)}$ and $\boldsymbol{\varepsilon}^{(2^*)}$ are already known, then two unknown variables, $\boldsymbol{\varepsilon}^{(1)}$ and $\boldsymbol{\varepsilon}^{(1)}$, can be solved with two equations in Eq. (3.3) theoretically. Finally, the total strain and stress can be derived with Eqs. (3.2) and (3.3).

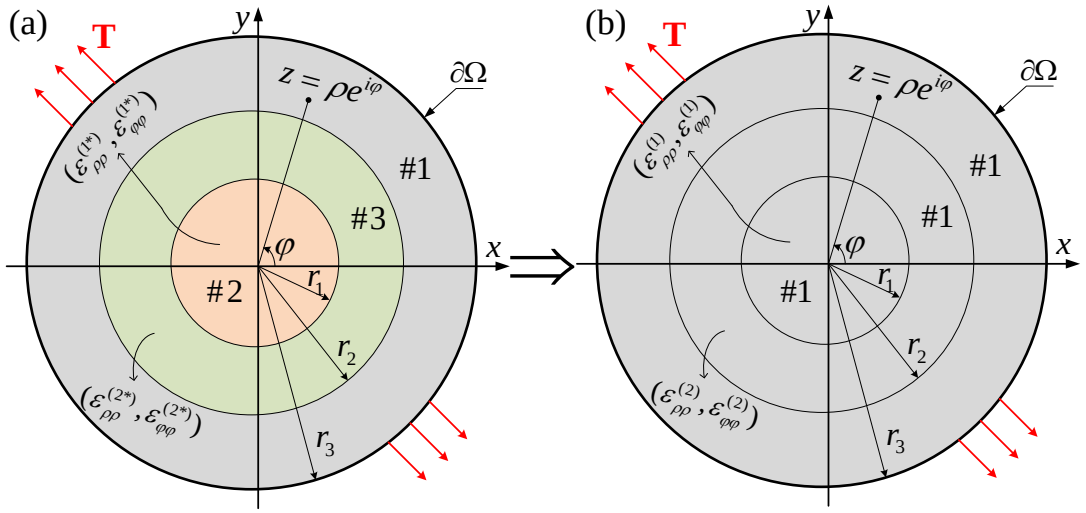

Fig. 4 A three-phase concentric inhomogeneous inclusion problem (a) is transformed into a corresponding homogeneous inclusion problem (b) with the equivalent eigenstrain principle. In Fig. 4a, #1, #2, and #3 represent different materials within the matrix, the circular zone, and the annular zone, respectively. $\boldsymbol{\varepsilon}^{(1*)}(\varepsilon_{\rho\rho}^{(1*)},\varepsilon_{\varphi\varphi}^{(1*)})$ and $\boldsymbol{\varepsilon}^{(2*)}(\varepsilon_{\rho\rho}^{(2*)},\varepsilon_{\varphi\varphi}^{(2*)})$ are original eigenstrains distributed in the circular and annular zones, respectively, in (a). $\boldsymbol{\varepsilon}^{(1)}(\varepsilon_{\rho\rho}^{(1)},\varepsilon_{\varphi\varphi}^{(1)})$ and $\boldsymbol{\varepsilon}^{(2)}(\varepsilon_{\rho\rho}^{(2)},\varepsilon_{\varphi\varphi}^{(2)})$ are equivalent eigenstrains within the circular and annular zones, respectively, in Fig. 4b. The two inclusion systems share identical total strain and stress distributions.

3.2. Solution for the inhomogeneous inclusion system

The concrete expressions for quantities that appear in Eq. (3.3) can be expressed as

$$\boldsymbol{\varepsilon}^{(1)}=\begin{bmatrix}\varepsilon_{\varphi\varphi}^{(1)}\\ \varepsilon_{\rho\rho}^{(1)}\\ \varepsilon_{\rho\varphi}^{(1)}\end{bmatrix},\ \boldsymbol{\varepsilon}^{(2)}=\begin{bmatrix}\varepsilon_{\varphi\varphi}^{(2)}\\ \varepsilon_{\rho\rho}^{(2)}\\ \varepsilon_{\rho\varphi}^{(2)}\end{bmatrix},\ \boldsymbol{\sigma}^{(1)}=\begin{bmatrix}\sigma_{\varphi\varphi}^{(1)}\\ \sigma_{\rho\rho}^{(1)}\\ \sigma_{\rho\varphi}^{(1)}\end{bmatrix},\ \boldsymbol{\sigma}^{(2)}=\begin{bmatrix}\sigma_{\varphi\varphi}^{(2)}\\ \sigma_{\rho\rho}^{(2)}\\ \sigma_{\rho\varphi}^{(2)}\end{bmatrix},$$

$$\boldsymbol{\varepsilon}^{(1*)}=\begin{bmatrix}\varepsilon_{\varphi\varphi}^{(1*)}\\ \varepsilon_{\rho\rho}^{(1*)}\\ \varepsilon_{\rho\varphi}^{(1*)}\end{bmatrix},\boldsymbol{\varepsilon}^{(2*)}=\begin{bmatrix}\varepsilon_{\varphi\varphi}^{(2*)}\\ \varepsilon_{\rho\rho}^{(2*)}\\ \varepsilon_{\rho\varphi}^{(2*)}\end{bmatrix},\mathbf{C}_1=\begin{bmatrix}\lambda_1+2\mu_1 & \lambda_1 & \\ \lambda_1 & \lambda_1+2\mu_1 & \\ & & 2\mu_1\end{bmatrix},\quad ,\qquad (3.4)$$

$$\mathbf{C}_2=\begin{bmatrix}\lambda_2+2\mu_2 & \lambda_2 & \\ \lambda_2 & \lambda_2+2\mu_2 & \\ & & 2\mu_2\end{bmatrix},\mathbf{C}_3=\begin{bmatrix}\lambda_3+2\mu_3 & \lambda_3 & \\ \lambda_3 & \lambda_3+2\mu_3 & \\ & & 2\mu_3\end{bmatrix}$$

where $\lambda_1=\mu_1(3-\kappa_1)/(1-\kappa_1)$, $\lambda_2=\mu_2(3-\kappa_2)/(1-\kappa_2)$, and $\lambda_3=\mu_3(3-\kappa_3)/(1-\kappa_3)$.

Eq. (3.3) can be rewritten as

$$\begin{cases}\boldsymbol{\varepsilon}^{(1)}=\left(\mathbf{C}_2^{-1}-\mathbf{C}_1^{-1}\right)\boldsymbol{\sigma}^{(1)}+\boldsymbol{\varepsilon}^{(1*)} & ,(0\le\rho<r_1)\\ \boldsymbol{\varepsilon}^{(2)}=\left(\mathbf{C}_3^{-1}-\mathbf{C}_1^{-1}\right)\boldsymbol{\sigma}^{(2)}+\boldsymbol{\varepsilon}^{(2*)} & ,(r_1\le\rho\le r_2)\end{cases}, \tag{3.5}$$

in which, $\boldsymbol{\sigma}^{(1)}$ and $\boldsymbol{\sigma}^{(2)}$ are shown as Eq. (2.8). Then by inserting Eqs. (2.8) and (3.4) into Eq. (3.5), the eigenstrains distributed in the circular and annular zones can be expressed as

$$\begin{cases}\varepsilon_{\varphi\varphi}^{(1)}=\dfrac{2\beta}{1-\alpha}\left[\displaystyle\int_{r_1}^{r_2}\frac{\left(\varepsilon_{\varphi\varphi}^{(2)}-\varepsilon_{\rho\rho}^{(2)}\right)}{r}dr+\int_{\rho}^{r_1}\frac{\left(\varepsilon_{\varphi\varphi}^{(1)}-\varepsilon_{\rho\rho}^{(1)}\right)}{r}dr\right]-\dfrac{2\alpha}{1-\alpha}\varepsilon_{\varphi\varphi}^{(1)}\\ +\dfrac{A}{4}\left[\dfrac{1-\kappa_1}{(\kappa_1-2)\mu_1}-\dfrac{1-\kappa_2}{(\kappa_1-2)\mu_2}\right]-\dfrac{2(\beta-\alpha)}{1-\alpha}\dfrac{1}{\rho^2}\displaystyle\int_0^{\rho}\left(\varepsilon_{\varphi\varphi}^{(1)}+\varepsilon_{\rho\rho}^{(1)}\right)rdr+\varepsilon_{\varphi\varphi}^{(1*)}\\ \varepsilon_{\rho\rho}^{(1)}=\dfrac{2\beta}{1-\alpha}\left[\displaystyle\int_{\rho}^{r_1}\frac{\left(\varepsilon_{\varphi\varphi}^{(1)}-\varepsilon_{\rho\rho}^{(1)}\right)}{r}dr+\int_{r_1}^{r_2}\frac{\left(\varepsilon_{\varphi\varphi}^{(2)}-\varepsilon_{\rho\rho}^{(2)}\right)}{r}dr\right]-\dfrac{2(2\beta-\alpha)}{1-\alpha}\varepsilon_{\varphi\varphi}^{(1)} & ,(\rho<r_1)\\ +\dfrac{A}{4}\left[\dfrac{1-\kappa_1}{(\kappa_1-2)\mu_1}-\dfrac{1-\kappa_2}{(\kappa_1-2)\mu_2}\right]+\dfrac{2(\beta-\alpha)}{1-\alpha}\dfrac{1}{\rho^2}\displaystyle\int_0^{\rho}\left(\varepsilon_{\varphi\varphi}^{(1)}+\varepsilon_{\rho\rho}^{(1)}\right)rdr+\varepsilon_{\rho\rho}^{(1*)}\\ \varepsilon_{\rho\varphi}^{(1)}=0\end{cases}, \tag{3.6a}$$

$$\begin{cases}\varepsilon_{\varphi\varphi}^{(2)}=\dfrac{A}{4}\left[\dfrac{1-\kappa_1}{(\kappa_1-2)\mu_1}-\dfrac{1-\kappa_2}{(\kappa_1-2)\mu_2}\right]+\varepsilon_{\varphi\varphi}^{(2*)}+\dfrac{2\beta_1}{1-\alpha_1}\displaystyle\int_{\rho}^{r_2}\frac{\left(\varepsilon_{\varphi\varphi}^{(2)}-\varepsilon_{\rho\rho}^{(2)}\right)}{r}dr\\ -\dfrac{2(\beta_1-\alpha_1)}{1-\alpha_1}\dfrac{1}{\rho^2}\left[\displaystyle\int_0^{r_1}\left(\varepsilon_{\varphi\varphi}^{(1)}+\varepsilon_{\rho\rho}^{(1)}\right)rdr+\int_{r_1}^{\rho}\left(\varepsilon_{\varphi\varphi}^{(2)}+\varepsilon_{\rho\rho}^{(2)}\right)rdr\right]-\dfrac{2\alpha_1}{1-\alpha_1}\varepsilon_{\varphi\varphi}^{(2)}\\ \varepsilon_{\rho\rho}^{(2)}=\dfrac{A}{4}\left[\dfrac{1-\kappa_1}{(\kappa_1-2)\mu_1}-\dfrac{1-\kappa_2}{(\kappa_1-2)\mu_2}\right]+\varepsilon_{\rho\rho}^{(2*)}+\dfrac{2\beta_1}{1-\alpha_1}\displaystyle\int_{\rho}^{r_2}\frac{\left(\varepsilon_{\varphi\varphi}^{(2)}-\varepsilon_{\rho\rho}^{(2)}\right)}{r}dr & ,(r_1\le\rho\le r_2),\\ +\dfrac{2(\beta_1-\alpha_1)}{1-\alpha_1}\dfrac{1}{\rho^2}\left[\displaystyle\int_0^{r_1}\left(\varepsilon_{\varphi\varphi}^{(1)}+\varepsilon_{\rho\rho}^{(1)}\right)rdr+\int_{r_1}^{\rho}\left(\varepsilon_{\varphi\varphi}^{(2)}+\varepsilon_{\rho\rho}^{(2)}\right)rdr\right]-\dfrac{2(2\beta_1-\alpha_1)}{1-\alpha_1}\varepsilon_{\varphi\varphi}^{(2)}\\ \varepsilon_{\rho\varphi}^{(2)}=0\end{cases} \tag{3.6b}$$

where α, β, α_1, and β_1 are Dundurs' constants (Dundurs, 1969):

$$\begin{aligned}\alpha&=\frac{\mu_1(\kappa_2+1)-\mu_2(\kappa_1+1)}{\mu_1(\kappa_2+1)+\mu_2(\kappa_1+1)},\beta=\frac{\mu_1(\kappa_2-1)-\mu_2(\kappa_1-1)}{\mu_1(\kappa_2+1)+\mu_2(\kappa_1+1)}\\ \alpha_1&=\frac{\mu_1(\kappa_3+1)-\mu_3(\kappa_1+1)}{\mu_1(\kappa_3+1)+\mu_3(\kappa_1+1)},\beta_1=\frac{\mu_1(\kappa_3-1)-\mu_3(\kappa_1-1)}{\mu_1(\kappa_3+1)+\mu_3(\kappa_1+1)}\end{aligned}. \tag{3.7}$$

In order to derive the equivalent eigenstrains $(\varepsilon_{\varphi\rho}^{(1)},\varepsilon_{\rho\rho}^{(1)},\varepsilon_{\varphi\varphi}^{(2)},\varepsilon_{\rho\rho}^{(2)})$ more easily. We

transform Eq. (3.6) into

$$\begin{cases} \varepsilon_{\varphi\varphi}^{(1)}+\varepsilon_{\rho\rho}^{(1)}=\varepsilon_{\varphi\varphi}^{(1*)}+\varepsilon_{\rho\rho}^{(1*)}+\dfrac{A}{2}\left[\dfrac{1-\kappa_1}{(\kappa_1-2)\mu_1}-\dfrac{1-\kappa_2}{(\kappa_2-2)\mu_2}\right] \\ +\dfrac{4\beta}{1-\alpha}\left[\int_\rho^{r_1}\dfrac{\left(\varepsilon_{\varphi\varphi}^{(1)}-\varepsilon_{\rho\rho}^{(1)}\right)}{r}dr+\int_{r_1}^{r_2}\dfrac{\left(\varepsilon_{\varphi\varphi}^{(2)}-\varepsilon_{\rho\rho}^{(2)}\right)}{r}dr-\varepsilon_{\varphi\varphi}^{(1)}\right] \qquad ,(\rho<r_1) \\ \varepsilon_{\varphi\varphi}^{(1)}-\varepsilon_{\rho\rho}^{(1)}=\dfrac{4(\beta-\alpha)}{1-\alpha}\left[-\dfrac{1}{\rho^2}\int_0^{\rho}\left(\varepsilon_{\varphi\varphi}^{(1)}+\varepsilon_{\rho\rho}^{(1)}\right)rdr+\varepsilon_{\varphi\varphi}^{(1)}\right]+\varepsilon_{\varphi\varphi}^{(1*)}-\varepsilon_{\rho\rho}^{(1*)} \end{cases}$$

$$\begin{cases} \varepsilon_{\varphi\varphi}^{(2)}+\varepsilon_{\rho\rho}^{(2)}=\dfrac{4\beta_1}{1-\alpha_1}\left[\int_\rho^{r_2}\dfrac{\left(\varepsilon_{\varphi\varphi}^{(2)}-\varepsilon_{\rho\rho}^{(2)}\right)}{r}dr-\varepsilon_{\varphi\varphi}^{(2)}\right]+\dfrac{A}{2}\left[\dfrac{1-\kappa_1}{(\kappa_1-2)\mu_1}-\dfrac{1-\kappa_2}{(\kappa_2-2)\mu_2}\right]+\varepsilon_{\varphi\varphi}^{(2*)}+\varepsilon_{\rho\rho}^{(2*)} \\ \varepsilon_{\varphi\varphi}^{(2)}-\varepsilon_{\rho\rho}^{(2)}=-\dfrac{4(\beta_1-\alpha_1)}{1-\alpha_1}\left\{\dfrac{1}{\rho^2}\left[\int_0^{r_1}\left(\varepsilon_{\varphi\varphi}^{(1)}+\varepsilon_{\rho\rho}^{(1)}\right)rdr+\int_{r_1}^{\rho}\left(\varepsilon_{\varphi\varphi}^{(2)}+\varepsilon_{\rho\rho}^{(2)}\right)rdr\right]-\varepsilon_{\varphi\varphi}^{(2)}\right\}+\varepsilon_{\varphi\varphi}^{(2*)}-\varepsilon_{\rho\rho}^{(2*)} \end{cases}$$

$$,(r_1\le\rho\le r_2)$$

.(3.8)

Then by letting

$$\begin{aligned} \varepsilon_d^{(1)}&=\varepsilon_{\varphi\varphi}^{(1)}-\varepsilon_{\rho\rho}^{(1)} \quad \varepsilon_s^{(1)}=\varepsilon_{\varphi\varphi}^{(1)}+\varepsilon_{\rho\rho}^{(1)} \\ \varepsilon_d^{(2)}&=\varepsilon_{\varphi\varphi}^{(2)}-\varepsilon_{\rho\rho}^{(2)} \quad \varepsilon_s^{(2)}=\varepsilon_{\varphi\varphi}^{(2)}+\varepsilon_{\rho\rho}^{(2)} \end{aligned}. \tag{3.9}$$

Eq. (3.8) can be rewritten as

$$\begin{cases} \dfrac{1+\alpha-2\beta}{1-\alpha}\rho^2\varepsilon_d^{(1)}+\dfrac{2(\beta-\alpha)}{1-\alpha}\left(2\int_0^{\rho}\varepsilon_s^{(1)}rdr-\rho^2\varepsilon_s^{(1)}\right)=\rho^2\left(\varepsilon_{\varphi\varphi}^{(1*)}-\varepsilon_{\rho\rho}^{(1*)}\right) \\ \varepsilon_s^{(1)}+\dfrac{2\beta}{1-\alpha}\left(\varepsilon_s^{(1)}+\varepsilon_d^{(1)}-2\int_\rho^{r_1}\dfrac{\varepsilon_d^{(1)}}{r}dr-2\int_{r_1}^{r_2}\dfrac{\varepsilon_d^{(2)}}{r}dr\right)=\varepsilon_{\varphi\varphi}^{(1*)}+\varepsilon_{\rho\rho}^{(1*)}+\dfrac{A}{2}\left[\dfrac{1-\kappa_1}{(\kappa_1-2)\mu_1}-\dfrac{1-\kappa_2}{(\kappa_2-2)\mu_2}\right] \end{cases}$$

$$\begin{cases} \dfrac{1+\alpha_1-2\beta_1}{1-\alpha_1}\rho^2\varepsilon_d^{(2)}+\dfrac{2(\beta_1-\alpha_1)}{1-\alpha_1}\left(2\int_{r_1}^{\rho}\varepsilon_s^{(2)}rdr+2\int_0^{r_1}\varepsilon_s^{(1)}rdr-\rho^2\varepsilon_s^{(2)}\right)=\rho^2\left(\varepsilon_{\varphi\varphi}^{(2*)}-\varepsilon_{\rho\rho}^{(2*)}\right) \\ \varepsilon_s^{(2)}+\dfrac{2\beta_1}{1-\alpha_1}\left(\varepsilon_s^{(2)}+\varepsilon_d^{(2)}-2\int_\rho^{r_2}\dfrac{\varepsilon_d^{(2)}}{r}dr\right)=\left(\varepsilon_{\varphi\varphi}^{(2*)}+\varepsilon_{\rho\rho}^{(2*)}\right)+\dfrac{A}{2}\left[\dfrac{1-\kappa_1}{(\kappa_1-2)\mu_1}-\dfrac{1-\kappa_2}{(\kappa_2-2)\mu_2}\right] \end{cases}$$

.(3.10)

And the equivalent eigenstrains can be obtained from the equation sets of Eq. (3.10). After some calculations similar to our previous work (Yan *et al.*, 2022), we can obtain the eigenstrain distributions as

$$\begin{cases} \varepsilon_{\varphi\varphi}^{(1)} = \dfrac{\varepsilon_{\varphi\varphi}^{(1*)}}{1+\alpha} + \dfrac{\alpha-2\beta}{1+\alpha}\varepsilon_{\rho\rho}^{(1*)} - \dfrac{\beta}{1+\alpha}\displaystyle\int \frac{\left[\rho^2\left(\varepsilon_{\varphi\varphi}^{(1*)} - \varepsilon_{\rho\rho}^{(1*)}\right)\right]_{,\rho}}{\rho^2} d\rho - \\ \qquad \dfrac{\alpha-\beta}{1+\alpha}\dfrac{1}{\rho^2}\displaystyle\int \rho^2\left(\varepsilon_{\varphi\varphi}^{(1*)} + \varepsilon_{\rho\rho}^{(1*)}\right)_{,\rho} d\rho + \frac{1}{2}\left(C_1 + \frac{C_2}{\rho^2}\right) \\ \varepsilon_{\rho\rho}^{(1)} = \dfrac{\alpha-2\beta}{1+\alpha}\varepsilon_{\varphi\varphi}^{(1*)} + \dfrac{\varepsilon_{\rho\rho}^{(1*)}}{1+\alpha} - \dfrac{\beta}{1+\alpha}\displaystyle\int \frac{\left[\rho^2\left(\varepsilon_{\varphi\varphi}^{(1*)} - \varepsilon_{\rho\rho}^{(1*)}\right)\right]_{,\rho}}{\rho^2} d\rho + \\ \qquad \dfrac{\alpha-\beta}{1+\alpha}\dfrac{1}{\rho^2}\displaystyle\int \rho^2\left(\varepsilon_{\varphi\varphi}^{(1*)} + \varepsilon_{\rho\rho}^{(1*)}\right)_{,\rho} d\rho + \frac{1}{2}\left(C_1 - \frac{C_2}{\rho^2}\right) \end{cases} \quad ,(3.11a)$$

$$\begin{cases} \varepsilon_{\varphi\varphi}^{(2)} = \dfrac{\varepsilon_{\varphi\varphi}^{(2*)}}{1+\alpha_1} + \dfrac{\alpha_1-2\beta_1}{1+\alpha_1}\varepsilon_{\rho\rho}^{(2*)} - \dfrac{\beta_1}{1+\alpha_1}\displaystyle\int \frac{\left[\rho^2\left(\varepsilon_{\varphi\varphi}^{(2*)} - \varepsilon_{\rho\rho}^{(2*)}\right)\right]_{,\rho}}{\rho^2} d\rho - \\ \qquad \dfrac{\alpha_1-\beta_1}{1+\alpha_1}\dfrac{1}{\rho^2}\displaystyle\int \rho^2\left(\varepsilon_{\varphi\varphi}^{(2*)} + \varepsilon_{\rho\rho}^{(2*)}\right)_{,\rho} d\rho + \frac{1}{2}\left(C_3 + \frac{C_4}{\rho^2}\right) \\ \varepsilon_{\rho\rho}^{(2)} = \dfrac{\alpha_1-2\beta_1}{1+\alpha_1}\varepsilon_{\varphi\varphi}^{(2*)} + \dfrac{\varepsilon_{\rho\rho}^{(2*)}}{1+\alpha_1} - \dfrac{\beta_1}{1+\alpha_1}\displaystyle\int \frac{\left[\rho^2\left(\varepsilon_{\varphi\varphi}^{(2*)} - \varepsilon_{\rho\rho}^{(2*)}\right)\right]_{,\rho}}{\rho^2} d\rho + \\ \qquad \dfrac{\alpha_1-\beta_1}{1+\alpha_1}\dfrac{1}{\rho^2}\displaystyle\int \rho^2\left(\varepsilon_{\varphi\varphi}^{(2*)} + \varepsilon_{\rho\rho}^{(2*)}\right)_{,\rho} d\rho + \frac{1}{2}\left(C_3 - \frac{C_4}{\rho^2}\right) \end{cases} \quad ,(3.11b)$$

where the concrete expressions of constant terms $C_i (i = 1,2,3,4)$ are determined by particular problems. C_1 and C_2 can be obtained by inserting Eq. (3.11a) into Eq. (3.10). Similarly, C_3 and C_4 can be obtained by inserting Eq. (3.11b) into Eq. (3.10). The two eigenstrain distributions share the same form obviously. Since the equivalent eigenstrains are already obtained as Eq. (3.11), the stress field can be simply derived from Eq. (2.8).

In this section, the general analytical solution of the stress field for the three-phase concentric inhomogeneous inclusion within a finite matrix is derived, and it is one of the key theoretical results in this paper. In the following sections, stress problems of ZTA reinforced metal matrix composites will be analyzed based on the fundamental solution developed in this section.

4. Problems with thermal-induced eigenstrains

In this section, a three-phase concentric model with eigenstrains aroused by thermal load will be analyzed. The stress response is caused by temperature change, which could occur in the manufacturing process or during service. With a temperature change ΔT, the thermal strains in different materials can be written as

$$\begin{cases} \varepsilon_T = \alpha_c\ \Delta T & \rho < r_1 \\ \varepsilon_T = \alpha_a\ \Delta T & r_1 \le \rho \le r_2 \\ \varepsilon_T = \alpha_m\ \Delta T & r_2 < \rho \le r_3 \end{cases}, \tag{4.1}$$

where α_c, α_a, and α_m are the thermal expand coefficients of materials residing in the circular zone, the annular zone and the matrix, respectively. In terms of the framework of eigenstrain theory, the eigenstrains due to thermal load can be written as

$$\begin{cases} \varepsilon_{\varphi\varphi}^{(1^*)} = \varepsilon_{\rho\rho}^{(1^*)} = \varepsilon^* = (\alpha_c - \alpha_m)\Delta T & \rho < r_1 \\ \varepsilon_{\varphi\varphi}^{(2^*)} = \varepsilon_{\rho\rho}^{(2^*)} = \varepsilon^{**} = (\alpha_a - \alpha_m)\Delta T & r_1 \le \rho \le r_2 \end{cases}, \tag{4.2}$$

and the matrix is equivalently regarded as eigenstrain-free. We will derive the stress distribution with known eigenstrain distributions of Eq. (4.2), and no other changes are made in the model. By inserting Eq. (4.2) into Eq. (3.11), the equivalent eigenstrains can be derived as

$$\begin{cases} \varepsilon_{\varphi\varphi}^{(1)} = \dfrac{1+\alpha-2\beta}{1+\alpha}\varepsilon^* + \dfrac{1}{2}\left(C_1 + \dfrac{C_2}{\rho^2}\right) \\ \varepsilon_{\rho\rho}^{(1)} = \dfrac{1+\alpha-2\beta}{1+\alpha}\varepsilon^* + \dfrac{1}{2}\left(C_1 - \dfrac{C_2}{\rho^2}\right) \end{cases}, \quad \begin{cases} \varepsilon_{\varphi\varphi}^{(2)} = \dfrac{1+\alpha_1-2\beta_1}{1+\alpha_1}\varepsilon^{**} + \dfrac{1}{2}\left(C_3 + \dfrac{C_4}{\rho^2}\right) \\ \varepsilon_{\rho\rho}^{(2)} = \dfrac{1+\alpha_1-2\beta_1}{1+\alpha_1}\varepsilon^{**} + \dfrac{1}{2}\left(C_3 - \dfrac{C_4}{\rho^2}\right) \end{cases}. \tag{4.3}$$

It is worth noting that the constant terms $C_i (i = 1,2,3,4)$ in Eq. (4.3) are unknown yet.

By inserting Eq. (4.3) into Eq. (3.10), we can obtain

$$\begin{cases} C_2 = 0 \\ \dfrac{1+\alpha_1-2\beta_1}{\beta_1-\alpha_1}C_4 = 2r_1^2\left[\dfrac{2(1+\alpha_1-2\beta_1)}{1+\alpha_1}\varepsilon^{**} + C_3\right] - 2r_1^2\left[\dfrac{2(1+\alpha-2\beta)}{1+\alpha}\varepsilon^* + C_1\right] \\ \dfrac{1-\alpha+2\beta}{1-\alpha}\left[\dfrac{2(1+\alpha-2\beta)}{1+\alpha}\varepsilon^* + C_1\right] = 2\varepsilon^* - \dfrac{2C_4\beta}{1-\alpha}\left(\dfrac{1}{r_2^2} - \dfrac{1}{r_1^2}\right) + \dfrac{A}{2}\left[\dfrac{1-\kappa_1}{(\kappa_1-2)\mu_1} - \dfrac{1-\kappa_2}{(\kappa_2-2)\mu_2}\right] \\ \dfrac{1-\alpha_1+2\beta_1}{1-\alpha_1}\left[\dfrac{2(1+\alpha_1-2\beta_1)}{1+\alpha_1}\varepsilon^{**} + C_3\right] = 2\varepsilon^{**} - \dfrac{2\beta_1}{1-\alpha_1}\dfrac{C_4}{r_2^2} + \dfrac{A}{2}\left[\dfrac{1-\kappa_1}{(\kappa_1-2)\mu_1} - \dfrac{1-\kappa_2}{(\kappa_2-2)\mu_2}\right] \end{cases}, \tag{4.4}$$

in which, A can be expressed with eigenstrains as

$$A = \frac{2\mu_1}{(1+\kappa_1)}\frac{1}{r_3^2}\left\{\left[\frac{2(1+\alpha-2\beta)}{1+\alpha}\varepsilon^* + C_1\right]r_1^2 + \left(r_2^2 - r_1^2\right)\left[\frac{2(1+\alpha_1-2\beta_1)}{1+\alpha_1}\varepsilon^{**} + C_3\right]\right\}. \tag{4.5}$$

$C_i(i=1,2,3,4)$ can be derived with the equation set in Eq. (4.4). However, the explicit solutions are too lengthy, so they are not present here. With known constant terms $C_i(i=1,2,3,4)$, the stress field can also be derived by inserting Eq. (4.3) into Eq. (2.8) as

$$\begin{cases} \sigma_{\rho\rho} = -\dfrac{Ar_3^2}{\rho^2} + A \\ \sigma_{\varphi\varphi} = \dfrac{Ar_3^2}{\rho^2} + A \quad ,(r_2 < \rho < r_3)\,, \\ \sigma_{\rho\varphi} = 0 \end{cases} \tag{4.6a}$$

$$\begin{cases} \sigma_{\rho\rho} = -\dfrac{2\mu_1}{(1+\kappa_1)} \left\{ \begin{array}{l} C_4\left(\dfrac{1}{r_2^2} - \dfrac{1}{\rho^2}\right) + \dfrac{r_1^2}{\rho^2}\left[\dfrac{2(1+\alpha-2\beta)}{1+\alpha}\varepsilon^* + C_1\right] \\ +\left(1-\dfrac{r_1^2}{\rho^2}\right)\left[\dfrac{2(1+\alpha_1-2\beta_1)}{1+\alpha_1}\varepsilon^{**} + C_3\right] \end{array} \right\} + A \\ \sigma_{\varphi\varphi} = -\dfrac{2\mu_1}{(1+\kappa_1)} \left\{ \begin{array}{l} C_4\left(\dfrac{1}{r_2^2} + \dfrac{1}{\rho^2}\right) - \dfrac{r_1^2}{\rho^2}\left[\dfrac{2(1+\alpha-2\beta)}{1+\alpha}\varepsilon^* + C_1\right] \\ +\left(1+\dfrac{r_1^2}{\rho^2}\right)\left[\dfrac{2(1+\alpha_1-2\beta_1)}{1+\alpha_1}\varepsilon^{**} + C_3\right] \end{array} \right\} + A \quad ,(r_1 \le \rho \le r_2)\,, \\ \sigma_{\rho\varphi} = 0 \end{cases} \tag{4.6b}$$

$$\begin{cases} \sigma_{\rho\rho} = -\dfrac{2\mu_1}{(1+\kappa_1)}\left[C_4\left(\dfrac{1}{r_2^2} - \dfrac{1}{r_1^2}\right) + \dfrac{2(1+\alpha-2\beta)}{1+\alpha}\varepsilon^* + C_1\right] + A \\ \sigma_{\varphi\varphi} = -\dfrac{2\mu_1}{(1+\kappa_1)}\left[C_4\left(\dfrac{1}{r_2^2} - \dfrac{1}{r_1^2}\right) + \dfrac{2(1+\alpha-2\beta)}{1+\alpha}\varepsilon^* + C_1\right] + A \quad ,(\rho < r_1)\,. \\ \sigma_{\rho\varphi} = 0 \end{cases} \tag{4.6c}$$

Eq. (4.6) is the general analytical solution of stress field for the three-phase concentric inclusion model with thermal-induced eigenstrains. Any composite materials that conform to the model can employ the analytical solution. In the next section, the model and its analytical solution will be utilized with concrete material parameters to analyze stress fields and accompanied phase transformation of zirconia in ZTA reinforced metal composite materials.

5. Application for ZTA reinforced metal matrix composites

This section will demonstrate how the stress fields of ZTA reinforced composites can be derived with the previous analytical solutions. The impact of transformation strain on the stress field is also investigated. Furthermore, the mechanism of zirconia as a stress buffer to relief extremely high stresses within it is discussed.

5.1. The normalized stress distribution of ZTA reinforced HCCI composite

The temperature change is still assumed to be ΔT, which means that the eigenstrains are the same as Eq. (4.2). The equivalent eigenstrains are shown in Eq. (4.3). Then the normalized stress distribution can be obtained from Eq. (4.6) by dividing $2\mu_1/\alpha_m\Delta T(1+\kappa_1)$ as

$$\begin{cases} \bar{\sigma}_{\rho\rho} = (1-\dfrac{1}{\bar{\rho}^2})\bar{A} \\ \bar{\sigma}_{\varphi\varphi} = (1+\dfrac{1}{\bar{\rho}^2})\bar{A} \end{cases}, (\frac{r_2}{r_3} < \bar{\rho} < 1), \tag{5.1a}$$

$$\begin{cases} \bar{\sigma}_{\rho\rho} = -\left\{ \begin{array}{l} \bar{C}_4(\dfrac{r_3^2}{r_2^2} - \dfrac{1}{\bar{\rho}^2}) + \dfrac{r_1^2}{r_3^2}\dfrac{1}{\bar{\rho}^2}\left[\dfrac{2(1+\alpha-2\beta)}{1+\alpha}\bar{\varepsilon}^{*} + \bar{C}_1\right] \\ +(1-\dfrac{r_1^2}{r_3^2}\dfrac{1}{\bar{\rho}^2})\left[\dfrac{2(1+\alpha_1-2\beta_1)}{1+\alpha_1}\bar{\varepsilon}^{**} + \bar{C}_3\right] \end{array} \right\} + \bar{A} \\ \bar{\sigma}_{\varphi\varphi} = -\left\{ \begin{array}{l} \bar{C}_4(\dfrac{r_3^2}{r_2^2} + \dfrac{1}{\bar{\rho}^2}) - \dfrac{r_1^2}{r_3^2}\dfrac{1}{\bar{\rho}^2}\left[\dfrac{2(1+\alpha-2\beta)}{1+\alpha}\bar{\varepsilon}^{*} + \bar{C}_1\right] \\ +(1+\dfrac{r_1^2}{r_3^2}\dfrac{1}{\bar{\rho}^2})\left[\dfrac{2(1+\alpha_1-2\beta_1)}{1+\alpha_1}\bar{\varepsilon}^{**} + \bar{C}_3\right] \end{array} \right\} + \bar{A} \end{cases}, (\frac{r_1}{r_3} \le \bar{\rho} \le \frac{r_2}{r_3}), \tag{5.1b}$$

$$\begin{cases} \bar{\sigma}_{\rho\rho} = -\left[\bar{C}_4(\dfrac{r_3^2}{r_2^2} - \dfrac{r_3^2}{r_1^2}) + \dfrac{2(1+\alpha-2\beta)}{1+\alpha}\bar{\varepsilon}^{*} + \bar{C}_1\right] + \bar{A} \\ \bar{\sigma}_{\varphi\varphi} = -\left[\bar{C}_4(\dfrac{r_3^2}{r_2^2} - \dfrac{r_3^2}{r_1^2}) + \dfrac{2(1+\alpha-2\beta)}{1+\alpha}\bar{\varepsilon}^{*} + \bar{C}_1\right] + \bar{A} \end{cases}, (\bar{\rho} < \frac{r_1}{r_3}). \tag{5.1c}$$

where $\bar{\sigma}_{\rho\rho}$ and $\bar{\sigma}_{\varphi\varphi}$ represent the normalized radial and hoop stresses, and

$$\begin{aligned} &\bar{\rho} = \frac{\rho}{r_3}, \bar{C}_1 = \frac{C_1}{\alpha_m\Delta T}, \bar{C}_3 = \frac{C_3}{\alpha_m\Delta T}, \bar{C}_4 = \frac{C_4}{\alpha_m\Delta T r_3^2}, \\ &\bar{\varepsilon}^{*} = \frac{\varepsilon^{*}}{\alpha_m\Delta T} = \frac{\alpha_c-\alpha_m}{\alpha_m}, \bar{\varepsilon}^{**} = \frac{\varepsilon^{**}}{\alpha_m\Delta T} = \frac{\alpha_a-\alpha_m}{\alpha_m}, \\ &\bar{A} = \frac{r_1^2}{r_3^2}\left[\frac{2(1+\alpha-2\beta)}{1+\alpha}\bar{\varepsilon}^{*} + \bar{C}_1\right] + \frac{r_2^2-r_1^2}{r_3^2}\left[\frac{2(1+\alpha_1-2\beta_1)}{1+\alpha_1}\bar{\varepsilon}^{**} + \bar{C}_3\right] \end{aligned}. \tag{5.2}$$

Material properties of components in ZTA reinforced HCCI composite are shown

in Table I. HCCI, zirconia, and 99.5%Al_2O_3 are materials #1, #2, and #3, separately situated in domains $r_2 < \rho < r_3$, $\rho < r_1$, and $r_1 < \rho < r_2$. It is obvious that the material proportion is controlled by radiuses in Fig. 2. In the case of plane strain, the relation of volume fraction of different components and radiuses can be expressed as

$$V_{\#1} : V_{\#2} : V_{\#3} = (r_3^2 - r_2^2) : r_1^2 : (r_2^2 - r_1^2). \tag{5.3}$$

Two different cases will be analyzed as follows:

(*i*) We suppose that the material proportion is V_{ZrO2}: $V_{95\%Al2O3}$: V_{HCCI} = 3: 7: 10. Then the ratio of radiuses r_1, r_2, and r_3 can be derived as

$$\frac{r_1}{r_3} = \sqrt{0.15},\ \frac{r_2}{r_3} = \sqrt{0.5}. \tag{5.4}$$

With Eqs. (4.2), (4.3) and (5.4), inserting material properties shown in Table I into Eq. (4.4), we can get the normalized constant terms as

$$\begin{cases} \bar{C}_1 = 0.0774673\bar{\varepsilon}^{*} + 0.20715\bar{\varepsilon}^{**} = 0.0774673\dfrac{\alpha_c - \alpha_m}{\alpha_m} + 0.20715\dfrac{\alpha_a - \alpha_m}{\alpha_m} \\ \bar{C}_3 = 0.0613989\bar{\varepsilon}^{*} + 0.162525\bar{\varepsilon}^{**} = 0.0613989\dfrac{\alpha_c - \alpha_m}{\alpha_m} + 0.162525\dfrac{\alpha_a - \alpha_m}{\alpha_m} \\ \bar{C}_4 = 0.133178\bar{\varepsilon}^{*} + 0.146868\bar{\varepsilon}^{**} = 0.133178\dfrac{\alpha_c - \alpha_m}{\alpha_m} + 0.146868\dfrac{\alpha_a - \alpha_m}{\alpha_m} \end{cases}. \tag{5.5}$$

And the normalized stress distribution can be obtained by inserting Eqs. (5.4) and (5.5) into Eq. (5.1) as

$$\begin{cases} \begin{cases} \bar{\sigma}_{\rho\rho} = -0.0310174 \\ \bar{\sigma}_{\varphi\varphi} = -0.0310174 \end{cases} & ,(\bar{\rho} < \dfrac{r_1}{r_3}) \\ \begin{cases} \bar{\sigma}_{\rho\rho} = 0.752689 - \dfrac{0.117556}{\bar{\rho}^2} \\ \bar{\sigma}_{\varphi\varphi} = 0.752689 + \dfrac{0.117556}{\bar{\rho}^2} \end{cases} & ,(\dfrac{r_1}{r_3} \le \bar{\rho} \le \dfrac{r_2}{r_3}) \\ \begin{cases} \bar{\sigma}_{\rho\rho} = -0.517577 + \dfrac{0.517577}{\bar{\rho}^2} \\ \bar{\sigma}_{\varphi\varphi} = 0.517577 + \dfrac{0.517577}{\bar{\rho}^2} \end{cases} & ,(\dfrac{r_2}{r_3} < \bar{\rho} < 1) \end{cases}. \tag{5.6}$$

The corresponding diagram is shown in Fig. 5a. The normalized analytical radial stress $\bar{\sigma}_{\rho\rho}$ is continuous at the interfaces between different phases while there are evident jumps for the normalized hoop stress $\bar{\sigma}_{\varphi\varphi}$. The normalized stress distribution in zirconia zone is uniform and compressive. The normalized analytical radial stress $\bar{\sigma}_{\rho\rho}$ decreases to zero at the boundary $\bar{\rho} = 1$.

(*ii*) We change the material proportion to V_{ZrO2}: $V_{95\%Al2O3}$: V_{HCCI} = 5: 5: 10. The ratio of radiuses r_1, r_2, and r_3 can be derived with Eq. (5.3) as

$$\frac{r_1}{r_3}=\sqrt{0.25},\ \frac{r_2}{r_3}=\sqrt{0.5}\,. \tag{5.7}$$

Similar to the above procedures, we can obtain the normalized stress distribution as

$$\begin{cases}\bar{\sigma}_{\rho\rho}=0.0627364\\ \bar{\sigma}_{\varphi\varphi}=0.0627364\end{cases},(\bar{\rho}<\frac{r_1}{r_3})$$

$$\begin{cases}\bar{\sigma}_{\rho\rho}=0.850878-\dfrac{0.197035}{\bar{\rho}^2}\\ \bar{\sigma}_{\varphi\varphi}=0.850878+\dfrac{0.197035}{\bar{\rho}^2}\end{cases},(\frac{r_1}{r_3}\le\bar{\rho}\le\frac{r_2}{r_3}) \tag{5.8}$$

$$\begin{cases}\bar{\sigma}_{\rho\rho}=-0.456807+\dfrac{0.456807}{\bar{\rho}^2}\\ \bar{\sigma}_{\varphi\varphi}=-0.456807-\dfrac{0.456807}{\bar{\rho}^2}\end{cases},(\frac{r_2}{r_3}<\bar{\rho}<1)$$

The corresponding diagram is shown in Fig. 5b. As can be seen from Fig. 5a and Fig. 5b, the general trend of two stress distributions in corresponding zones is similar for ZTA reinforced HCCI composites. For example, the normalized analytical stresses are both uniform in the circular zone where zirconia resides. However, the remarkable thing is that they are compressive and tensile, respectively, with different material proportions, which shows that the model is capable of simulating different stress environments.

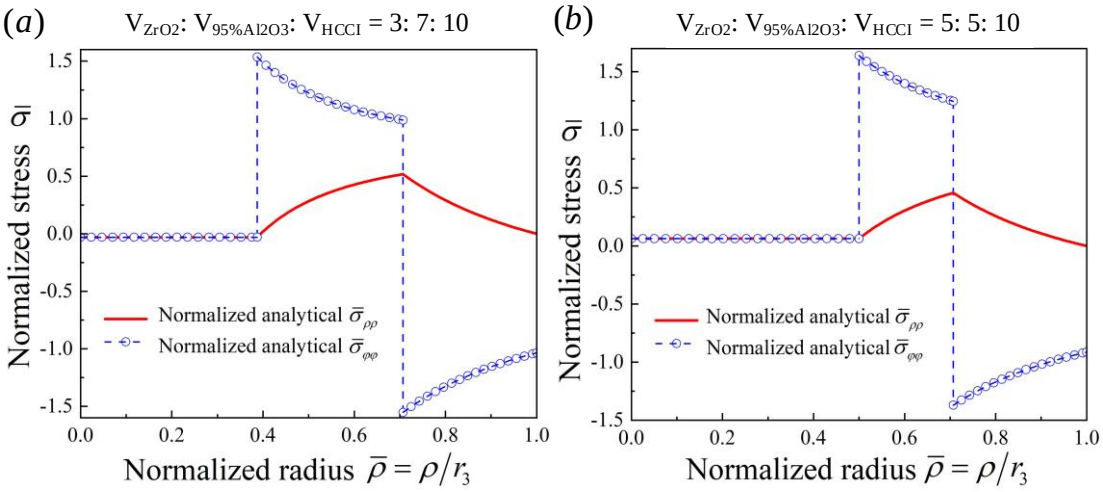

Fig. 5 The normalized radial and hoop stress distributions along normalized radius corresponding to the material proportions of V_{ZrO2}: $V_{95\%Al2O3}$: V_{HCCI} = 3: 7: 10 and V_{ZrO2}: $V_{95\%Al2O3}$: V_{HCCI} = 5: 5: 10, respectively.

Table I. Material properties of components in ZTA reinforced HCCI

Material properties	Material categories		
	99.5%Al_2O_3(#3)	ZrO_2(#2)	HCCI(#1)
Thermal expansion（α）×10^{-6}/℃	7.7	11	15
Elastic modulus（E）/GPa	370	210	220
Poisson's ratio（ν）	0.25	0.31	0.3

5.2. The stress distribution induced by transformation strain

During the process of preparation or service, transformation could take place in zirconia due to excessively high stress, and the transformation has an influence on the stress distribution of composites. In this part, we will demonstrate the influence of transformation strain on the three-phase concentric inclusion problems. We assume that the uniform transformation strain ε_T only exists in zirconia zone, then the eigenstrain distributions are taken as

$$\begin{cases} \varepsilon_{\varphi\varphi}^{(1^*)} = \varepsilon_{\rho\rho}^{(1^*)} = \varepsilon^* = \varepsilon_T & \rho < r_1 \\ \varepsilon_{\varphi\varphi}^{(2^*)} = \varepsilon_{\rho\rho}^{(2^*)} = \varepsilon^{**} = 0 & r_1 \le \rho \le r_2 \end{cases}. \tag{5.9}$$

By inserting Eq. (5.9) into Eq. (4.3), the equivalent eigenstrains can be obtained as

$$\begin{cases} \varepsilon_{\varphi\varphi}^{(1)} = \dfrac{(1+\alpha-2\beta)\varepsilon_T}{1+\alpha} + \dfrac{1}{2}\left(C_1 + \dfrac{C_2}{\rho^2}\right) \\ \varepsilon_{\rho\rho}^{(1)} = \dfrac{(1+\alpha-2\beta)\varepsilon_T}{1+\alpha} + \dfrac{1}{2}\left(C_1 - \dfrac{C_2}{\rho^2}\right) \end{cases}, \quad \begin{cases} \varepsilon_{\varphi\varphi}^{(2)} = \dfrac{1}{2}\left(C_3 + \dfrac{C_4}{\rho^2}\right) \\ \varepsilon_{\rho\rho}^{(2)} = \dfrac{1}{2}\left(C_3 - \dfrac{C_4}{\rho^2}\right) \end{cases}. \tag{5.10}$$

And constant terms $C_i (i = 1,2,3,4)$ can be derived with the equation set

$$\begin{cases} C_2 = 0 \\ \dfrac{1+\alpha_1-2\beta_1}{\beta_1-\alpha_1} C_4 = 2C_3 r_1^2 - 2r_1^2\left[\dfrac{2(1+\alpha-2\beta)}{1+\alpha}\varepsilon_T + C_1\right] \\ \dfrac{C_3(1-\alpha_1+2\beta_1)}{1-\alpha_1} + \dfrac{2\beta_1}{1-\alpha_1}\dfrac{C_4}{r_2^2} = \dfrac{A}{2}\left[\dfrac{1-\kappa_1}{(\kappa_1-2)\mu_1} - \dfrac{1-\kappa_2}{(\kappa_2-2)\mu_2}\right] \\ \dfrac{1-\alpha+2\beta}{1-\alpha}\left[\dfrac{2(1+\alpha-2\beta)}{1+\alpha}\varepsilon^* + C_1\right] = 2\varepsilon_T - \dfrac{2C_4\beta}{1-\alpha}\left(\dfrac{1}{r_2^2} - \dfrac{1}{r_1^2}\right) + \dfrac{A}{2}\left[\dfrac{1-\kappa_1}{(\kappa_1-2)\mu_1} - \dfrac{1-\kappa_2}{(\kappa_2-2)\mu_2}\right] \end{cases} \tag{5.11}$$

where

$$A = \frac{4\mu_1}{(1+\kappa_1)}\frac{1}{r_3^2}\left\{\frac{r_1^2}{2}\left[\frac{2(1+\alpha-2\beta)\varepsilon_T}{1+\alpha} + C_1\right] + \frac{C_3}{2}(r_2^2 - r_1^2)\right\}. \tag{5.12}$$

Inserting Eq. (5.9) into Eq. (4.6), the stress distribution can be expressed as

$$\begin{cases} \sigma_{\rho\rho} = -\dfrac{Ar_3^2}{\rho^2} + A \\ \sigma_{\varphi\varphi} = \dfrac{Ar_3^2}{\rho^2} + A \end{cases}, (r_2 < \rho < r_3), \tag{5.13a}$$

$$\begin{cases} \sigma_{\rho\rho} = -\dfrac{2\mu_1}{(1+\kappa_1)}\left\{C_4(\dfrac{1}{r_2^2} - \dfrac{1}{\rho^2}) + \dfrac{r_1^2}{\rho^2}\left[\dfrac{2(1+\alpha-2\beta)}{1+\alpha}\varepsilon_T + C_1\right] + (1-\dfrac{r_1^2}{\rho^2})C_3\right\} + A \\ \sigma_{\varphi\varphi} = -\dfrac{2\mu_1}{(1+\kappa_1)}\left\{C_4(\dfrac{1}{r_2^2} + \dfrac{1}{\rho^2}) - \dfrac{r_1^2}{\rho^2}\left[\dfrac{2(1+\alpha-2\beta)}{1+\alpha}\varepsilon_T + C_1\right] + (1+\dfrac{r_1^2}{\rho^2})C_3\right\} + A \end{cases}, (r_1 \le \rho \le r_2) \tag{5.13b}$$

$$\begin{cases} \sigma_{\rho\rho} = -\dfrac{2\mu_1}{(1+\kappa_1)}\left[C_4(\dfrac{1}{r_2^2} - \dfrac{1}{r_1^2}) + \dfrac{2(1+\alpha-2\beta)}{1+\alpha}\varepsilon_T + C_1\right] + A \\ \sigma_{\varphi\varphi} = -\dfrac{2\mu_1}{(1+\kappa_1)}\left[C_4(\dfrac{1}{r_2^2} - \dfrac{1}{r_1^2}) + \dfrac{2(1+\alpha-2\beta)}{1+\alpha}\varepsilon_T + C_1\right] + A \end{cases}, (\rho < r_1). \tag{5.13c}$$

Eq. (5.13) shows the general analytical solution of the stress distribution caused by the phase transformation of zirconia. If we suppose that $\varepsilon_T = 0.01$ and V_{ZrO2}: $V_{95\%Al2O3}$: V_{HCCI} = 3: 7: 10. Then with known material properties in Table I, the normalized stress distribution can be obtained from Eq. (5.13) by dividing $2\mu_1/(1+\kappa_1)$, as shown in Fig. 6.

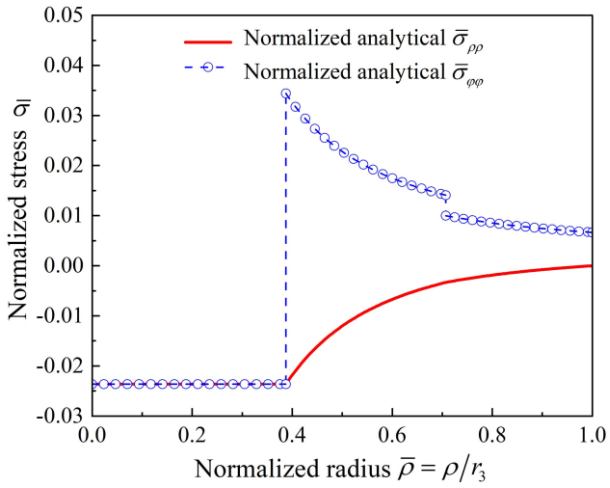

Fig. 6 Normalized stress distribution of ZTA reinforced HCCI composites induced by $\varepsilon_T = 0.01$. The material proportion is V_{ZrO2}: $V_{95\%Al2O3}$: V_{HCCI} = 3: 7: 10.

After the transformation, the compressive radial stress in the annular region can help

to reduce the radial stress in the alumina ceramic. If ε_T is set to -0.01, which means the monoclinic (m)→tetragonal (t) transformation occurs, the stress distribution will be opposite in sign to that shown in Fig. 6. Then the hoop compressive stress in the annular zone will cause a decrease in the hoop stress in the alumina ceramic, which allows more external tensile load applied. Therefore, the stress induced by transformation strain plays an important role in the toughening mechanism for ZTA reinforced metal matrix composites.

5.3. Thermal load induced transformation toughening in ZTA-reinforced metal matrix composites

The temperature change generates thermal eigenstrains, which will produce a stress $\sigma_{zirconia}$ in the zirconia zone. We suppose that the stress is tensile and it is high enough to trigger the phase transformation of zirconia (i.e. $\sigma_{zirconia} > \sigma_{CT}$, where σ_{CT} represents the known critical transformation stress of zirconia). It leads to the tetragonal (t)→monoclinic (m) transformation and produces a transformation strain (volume expansion) in the zirconia zone. This transformation process will continue until the stress in zirconia decreases to σ_{CT}. In the process, the stress induced by the transformation strain ε_T always helps to diminish the excessively high stress, which is believed to be the toughening mechanism of the composites due to the presence of zirconia. The actual stress distribution in the model is the sum of stresses caused by the thermal-induced eigenstrains and the transformation strain ε_T. Its general analytical solution can be obtained by the superposition of Eqs. (4.6) and (5.13). In terms of the basic toughening mechanism, by letting the actual stress equal to the known critical transformation stress σ_{CT}, the transformation strain ε_T can also be specified. Below, we will provide a specific example to illustrate how the transformation of zirconia relieves the excessively high stress in ZTA reinforced metal matrix composites caused by *thermal load*.

Now, suppose that a three-phase concentric inclusion in Fig. 2 is subjected to a thermal load ΔT. As shown in Eq. (5.1), the stress field induced by the *thermal load* is normalized by dividing term $2\mu_1/\alpha_m\Delta T(1+\kappa_1)$. By multiplying both sides of the equations obtained in Eq. (5.1) by the term $\alpha_m\Delta T$, we can obtain a newly normalized

form of the stress field, which is equivalently normalized by dividing term $2\mu_1/(1+\kappa_1)$. Take ZTA reinforced HCCI for example, assuming that the temperature drops from the phase transition temperature of zirconia at 950℃ to room temperature of 25℃, which means $\Delta T=-925$ ℃. The ratio between the radii is given as $r_1:r_2:r_3=3:8:10$. Then by multiplying term $\alpha_m\Delta T$ with Eq. (5.1), the newly normalized stress distribution caused by the *thermal load* (before the transformation) can be obtained as

$$\begin{cases}\bar{\sigma}_{\rho\rho}=0.00564693\\ \bar{\sigma}_{\varphi\varphi}=0.00564693\end{cases},(\bar{\rho}<\frac{r_1}{r_3})$$
$$\begin{cases}\bar{\sigma}_{\rho\rho}=-0.00744464+\dfrac{0.00117824}{\bar{\rho}^2}\\ \bar{\sigma}_{\varphi\varphi}=-0.00744464-\dfrac{0.00117824}{\bar{\rho}^2}\end{cases},(\frac{r_1}{r_3}\le\bar{\rho}\le\frac{r_2}{r_3}) \tag{5.14}$$
$$\begin{cases}\bar{\sigma}_{\rho\rho}=0.00996202-\dfrac{0.00996202}{\bar{\rho}^2}\\ \bar{\sigma}_{\varphi\varphi}=0.00996202+\dfrac{0.00996202}{\bar{\rho}^2}\end{cases},(\frac{r_2}{r_3}<\bar{\rho}<1)$$

It can be seen that the stress distribution in the zirconia is tensile and if it is greater than σ_{CT}, the tetragonal (t)→monoclinic (m) phase transformation will take place. We assume that zirconia undergoes a phase transformation strain of $\varepsilon_T=0.001$ to reduce the internal stress to the critical phase transformation stress. Similarly, the normalized stress distribution caused by ε_T can be obtained with Eq. (5.13) by dividing $2\mu_1/(1+\kappa_1)$. By superposing the result with Eq. (5.14), the stress distribution after the transformation can be obtained as

$$\begin{cases}\bar{\sigma}_{\rho\rho}=0.00251998\\ \bar{\sigma}_{\varphi\varphi}=0.00251998\end{cases},(\bar{\rho}<\frac{r_1}{r_3})$$
$$\begin{cases}\bar{\sigma}_{\rho\rho}=-0.00707735+\dfrac{0.00086376}{\bar{\rho}^2}\\ \bar{\sigma}_{\varphi\varphi}=-0.00707735-\dfrac{0.00086376}{\bar{\rho}^2}\end{cases},(\frac{r_1}{r_3}\le\bar{\rho}\le\frac{r_2}{r_3}) \tag{5.15}$$
$$\begin{cases}\bar{\sigma}_{\rho\rho}=0.0101826-\dfrac{0.0101826}{\bar{\rho}^2}\\ \bar{\sigma}_{\varphi\varphi}=0.0101826+\dfrac{0.0101826}{\bar{\rho}^2}\end{cases},(\frac{r_2}{r_3}<\bar{\rho}<1)$$

The stress distributions before and after the phase transformation are plotted in Fig. 7. It can be observed that, after phase transformation, the stress level in the zirconia

region decreases by approximately 50%, and the stress relief in the annular region is relatively significant, while the stress distribution in the matrix remains almost unchanged. The effect of stress relief shown in the circular and annular zone indicates the toughening effect attributed to the phase transformation.

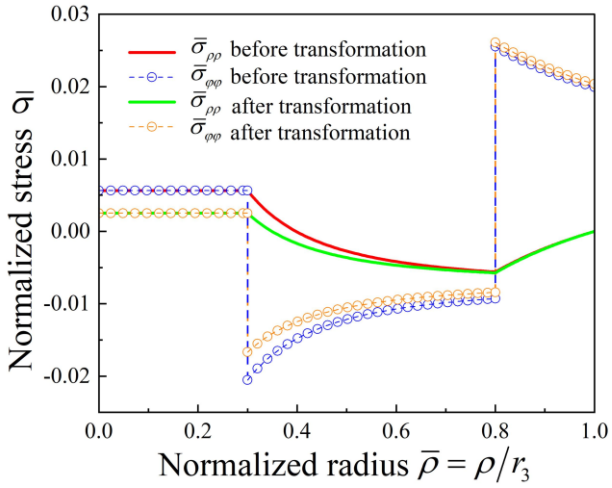

Fig. 7 The normalized stress distributions before and after phase transformation. The decrease of stress level in the zirconia and annular region after transformation is relatively significant.

In this section, the ZTA reinforced HCCI composite material is studied with the mechanical model established in §4. With known initial eigenstrains and material proportion, the normalized stress distribution is obtained. The general stress distribution caused purely by the transformation strain is also derived. With the above results, the transformation toughening mechanism of ZTA reinforced metal matrix composites is discussed.

6. Concluding remarks

In this paper, to study ZTA reinforced metal matrix composites, a three-phase concentric model with finite matrix has been proposed. Its general analytical solution has been derived with the equivalent eigenstrain principle and the superposition principle. Then based on the general analytical solution, the influence of thermal strains and transformation strains on the general stress distribution has been analyzed. Finally, two concrete examples of ZTA reinforced HCCI composites have been given to demonstrate the toughening mechanism due to the transformation of zirconia. All the results may be helpful in understanding the transformation toughening mechanism and designing the composites.

It is expected that the solutions developed in this paper can be useful for the further

modeling impact abrasive wear behavior of particle reinforced metal matrix composites elsewhere.

CRediT authorship contribution statement

Jiyang Yan formulated the problem, conducted the theoretical work, and drafted the manuscript. **Lifeng Ma** conceived the idea, supervised the work, and revised and edited the manuscript. **Juan Wang** performed the experimental work, participated the result analysis, revised and edited the manuscript. All authors gave their final approval for publication.

Declaration of competing interest

The authors declare that they have no known competing financial interests or personal relationships that could have appeared to influence the work reported in this paper.

Data availability

Data will be made available on request.

Acknowledgments

This work was partially supported by National Natural Science Foundation of China (Grant Nos. 12072254). L.M. would like to thank the support of the Sir Joseph Pope Fellowship from Nottingham University, UK. J.W. appreciates the support of National Key R&D Program of China (Grant No.2021YFB3701204) and GDAS' Project of Science and Technology Development (Grant No.2022GDASZH-2022010103).

References

Dundurs, J., 1969. Discussion:“Edge-bonded dissimilar orthogonal elastic wedges under normal and shear loading”(Bogy, DB, 1968, ASME J. Appl. Mech., 35, pp. 460–466).

Fan, L., Wang, Q., Yang, P., Chen, H., Hong, H., Zhang, W., Ren, J., 2018. Preparation of nickel coating on ZTA particles by electroless plating. Ceram. Int. 44, 11013–11021.

Fernie, J.A., Drew, R.A.L., Knowles, K.M., 2009. Joining of engineering ceramics. Int. Mater. Rev. 54, 283–331.

Gao, Q., Lu, Z., Jia, L., Wang, Y., 2022. Effect of B4C on wear behaviour of ZTA ceramic reinforced high chromium cast iron matrix composites. Mater. Sci. Technol. 38, 1474–1481.

Garvie, R.C., Hannink, R.H., Pascoe, R.T., 1975. Ceramic steel? Nature 258, 703–704.

Hannink, R.H.J., Kelly, P.M., Muddle, B.C., 2000. Transformation toughening in zirconia-containing ceramics. J. Am. Ceram. Soc. 83, 461–487.

Harris, S.J., 1988. Cast metal matrix composites. Mater. Sci. Technol. 4, 231–239.

He, H., Jiang, Y., Ru, J., Hua, Y., 2022. Nanoindentation and microstructure of interfacial layer in Ni-NiTi coated zirconia toughened alumina particles reinforced high chromium cast iron matrix composites. Mater. Lett. 311, 131561.

Heuer, A.H., 1987. Transformation toughening in ZrO2-containing ceramics. J. Am. Ceram. Soc. 70, 689–698.

Hill, H., Weber, S., Siebert, S., Theisen, W., 2011. Investigation of corrosion and wear properties of Fe based metal matrix composites consolidated by sintering and hot isostatic pressing. Powder Metall. 54, 455–462.

Kambakas, K., Tsakiropoulos, P., 2005. Solidification of high-Cr white cast iron–WC particle reinforced composites. Mater. Sci. Eng. A 413, 538–544.

Li, C., Li, Yefei, Shi, J., Li, B., Gao, Y., Goei, R., Li, Yuehui, Shah, I.A., Wu, K., Zhao, S., 2022. Interfacial characterization and erosive wear performance of zirconia toughened alumina ceramics particles reinforced high chromium white cast irons composites. Tribol. Int. 165, 107262.

Li, Y., Li, C., Tang, S., Zheng, Q., Wang, J., Zhang, Z., Wang, Z., 2019. Interfacial bonding and abrasive wear behavior of iron matrix composite reinforced by ceramic particles. Materials (Basel). 12, 3646.

Li, Z., Jiang, Y., Zhou, Rong, Lu, D., Zhou, Rongfeng, 2007. Dry three-body abrasive wear behavior of WC reinforced iron matrix surface composites produced by V-EPC infiltration casting process. Wear 262, 649–654.

Ma, D., Chen, H., Cheng, X., Gao, K., Wang, L., Zhang, L., Wang, H., Zhang, R., Lu, H., 2019. Preparation and properties of ZTA ceramics using blast furnace slag as

sintering additives. Mater. Res. Express 6, 65201.

Ma, L., Korsunsky, A.M., 2022. The Fundamental Formulation for Inhomogeneous Inclusion Problems with the Equivalent Eigenstrain Principle. Metals (Basel). 12, 582.

Ma, L., Korsunsky, A.M., 2014. The principle of equivalent eigenstrain for inhomogeneous inclusion problems. Int. J. Solids Struct. 51, 4477–4484.

Ma, X., Li, L., Zhang, F., Zhang, Z., Wang, H., Wang, E., 2018. Microstructure and wear characteristics of ATZ ceramic particle reinforced gray iron matrix surface composites. China Foundry 15, 167–172.

Miracle, D.B., 2005. Metal matrix composites–from science to technological significance. Compos. Sci. Technol. 65, 2526–2540.

Pagounis, E., Lindroos, V.K., 1998. Processing and properties of particulate reinforced steel matrix composites. Mater. Sci. Eng. A 246, 221–234.

Qin, Y., Wang, Y., Miao, W., Yang, P., Fu, D., Fan, L., Chen, H., 2022. Interface modification and impact abrasive wear behavior of ZTA particle-reinforced iron-matrix composite. Wear 490, 204205.

Qiu, B., Xing, S., Dong, Q., 2019. Fabrication and wear behavior of ZTA particles reinforced iron matrix composite produced by flow mixing and pressure compositing. Wear 428, 167–177.

Qiu, B., Xing, S.M., Dong, Q., 2017. Wear behaviour of iron matrix composite reinforced by ZTA particles in impact abrasion, in: IOP Conference Series: Materials Science and Engineering. IOP Publishing, p. 12028.

Ru, J., He, H., Jiang, Y., Zhou, R., Hua, Y., 2019a. Ionic Liquid-Assisted Preparation of Ni–Cr Dual Wrapped ZTA Particles for Reinforced Iron-Based Composites. Adv. Eng. Mater. 21, 1801120.

Ru, J., He, H., Jiang, Y., Zhou, R., Hua, Y., 2019b. Wettability and interaction mechanism for Ni-modified ZTA particles reinforced iron matrix composites. J. Alloys Compd. 786, 321–329.

Ru, J, Jia, Y., Jiang, Y., Feng, J., Zhou, R., Hua, Y., Wang, D., 2017. Modification of ZTA particles with Ni coating by electroless deposition. Surf. Eng. 33, 353–361.

Ru, Juanjian, Jiang, Y., Zhou, R., Feng, J., Hua, Y., Yang, Q., 2017. Preparation of Ni-Encapsulated ZTA Particles as Precursors to Reinforce Iron-Based Composites. Adv. Eng. Mater. 19, 1700268.

Sui, Y., Zhou, M., Jiang, Y., 2018. Characterization of interfacial layer of ZTA ceramic particles reinforced iron matrix composites. J. Alloys Compd. 741, 1169–1174.

Tang, S.L., Gao, Y.M., Li, Y.F., 2014. Recent developments in fabrication of ceramic particle reinforced iron matrix wear resistant surface composite using infiltration casting technology. Ironmak. Steelmak. 41, 633–640.

Wang, B., Zhao, W., Ma, L., 2020. Analysis of a finite matrix with an inhomogeneous circular inclusion subjected to a non-uniform eigenstrain. Arch. Appl. Mech. 90, 945–956.

Wang, J., Stevens, R., 1989. Zirconia-toughened alumina (ZTA) ceramics. J. Mater. Sci. 24, 3421–3440.

Wang, S., Sun, Y., Li, G., 2022. Study on cobalt coating on ZTA particles by electroless plating and impact-abrasive wear behavior of ZTAp reinforced iron matrix composite. Wear 510, 204489.

Wang, W.L., Liu, H.Y., Wang, X.J., 2020. Research progress in ZTA ceramic/iron matrix composites prepared by infiltration method. Spec. Cast. Nonferrous Alloy. 40, 37–41.

Wang, Y., Qin, Y., Fu, D., Chen, H., Pan, Y., Zhu, C., Yao, F., 2020. Behaviors of ZTA (zirconia toughened alumina) reinforced iron composites under impact abrasive wear conditions. Wear 458, 203397.

Xue, D., Jia, Y., Zhang, X., Jiang, Y., Sui, Y., 2019. Effect of ZTA volume fractions on the microstructure and properties of ZTAp/high manganese steel composites. Mater. Res. Express 6, 46535.

Yan, J., Zhu, J., Ma, L., 2022. Analytical solutions for coated circular inhomogeneity with non-uniform axisymmetric eigenstrain distribution. Int. J. Solids Struct. 243, 111567.

Zeng, H., Sui, Y., Niu, G., He, H., Jiang, Y., Zhou, M., 2021. Effect of alloy powder

on the properties of ZTA particles reinforced high chromium cast iron composites. Mater. Res. Express 8, 36509.

Zheng, B., Li, W., Tu, X., Song, S., Huang, W., 2019. Effect of ZTA ceramic particles strengthened high chromium white cast iron on three-body abrasion behavior. Mater. Res. Express 6, 116581.

Zheng, K., Gao, Y., Li, Y., Zhao, S., Wang, J., 2014. Three-body abrasive wear resistance of iron matrix composites reinforced with ceramic particles. Proc. Inst. Mech. Eng. Part J J. Eng. Tribol. 228, 3–10.

Zhou, M., Jiang, Y., Sui, Y., 2019. Microstructure and properties of interfacial transition zone in ZTA particle–reinforced iron composites. Appl. Phys. A 125, 1–10.